Interference between geothermal doublets across a fault under subsurface uncertainty Implications for field development and regulation

Daniilidis, Alexandros; Nick, Hamidreza M.; Bruhn, David F.

DOI
10.1016/j.geothermics.2021.102041

Publication date
2021

Document Version
Final published version

Published in
Geothermics

Citation (APA)
Daniilidis, A., Nick, H. M., & Bruhn, D. F. (2021). Interference between geothermal doublets across a fault under subsurface uncertainty: Implications for field development and regulation. *Geothermics*, *91*, 1-22. Article 102041. https://doi.org/10.1016/j.geothermics.2021.102041

Geothermics 91 (2021) 102041

Contents lists available at ScienceDirect

Geothermics

journal homepage: www.elsevier.com/locate/geothermics

Interference between geothermal doublets across a fault under subsurface uncertainty; implications for field development and regulation

Alexandros Daniilidis [a,*], Hamidreza M. Nick [b], David F. Bruhn [a,c]

[a] Delft University of Technology, Stewinweg 1, Delft 2628CN, The Netherlands
[b] Technical University of Denmark, 2800 Kgs. Lyngby, Denmark
[c] GFZ German Research Centre for Geosciences, Telegrafenberg, Potsdam, Germany

ARTICLE INFO

Keywords:
Geothermal doublet interference
Fault
NPV
Lifetime
Heat in Place (HIP) recovery
Uncertainty

ABSTRACT

Direct Use Geothermal Systems (DUGS) are increasing their installed capacity worldwide and denser developments with multiple doublets are becoming more common. Interference between doublets therefore becomes an additional concern to subsurface uncertainties. Faults can be either barriers or conduits to flow and can affect the fluid pathways inside the reservoir. The interference between two doublets that are separated by a fault has not been previously studied for DUGS. In this work considering subsurface uncertainty in a full factorial design using 5184 3D reservoir simulations we show that a fault can reduce the system lifetime of a two-doublet system by more than 40 % if one doublet is at close proximity to it. Further, we identify that the fault can also improve both the system lifetime and generated Net Present Value (NPV) with appropriate development decisions. Contrary to previous results that did not consider reservoir architecture, a tramline well configuration is preferable when the doublets have the fault in the centre, while a checkerboard configuration is preferable as the distance to the fault decreases. The Heat In Place (HIP) recovery shows a linear relationship with flow rate and well spacing that is not affected by the fault distance or flow properties. The dimensions of the Influence Area (IA) previously considered are insufficient to capture the temperature drop at the producer wells and the fault position can increase this discrepancy. Our results show the importance of fault characterisation and well positioning with respect to a fault considering subsurface uncertainty and how this can affect denser field development of DUGS. Our findings suggest to integrate faults and the relative positioning of well doublets with respect to a fault more strongly in field development plans. Such considerations should also be included in future optimization plans of multi-well geothermal systems. Moreover, the regulatory framework should be revised to achieve a better match between the IA boundary and the production well temperature drop to enable better planning for denser development of DUGS.

1. Introduction

Direct Use Geothermal Systems (DUGS) are rapidly increasing both in terms of installed capacity, as well as in energy generation at a global level (Lund and Toth, 2020). This increased contribution is also moving toward city landscapes (Yan et al., 2017), contributing to an energy supply with a reduced carbon footprint (Anderson and Rezaie, 2019). Countries such as the Netherlands have set ambitious plans for further developing geothermal energy in the coming years (Schoof et al., 2018). As the demand for renewable, low carbon energy from DUGS is increasing, spatial coordination of the developments will be required (Willems and Nick, 2019). In such a context, interference between systems can influence the overall system lifetime and generated Net Present Value (Willems et al., 2017b). A geothermal doublet, comprised of one injector and one producer well, is most often used as the simplest form of deep DUGS (Barbier, 2002; Daniilidis et al., 2016; Saeid et al., 2015). For a single doublet, proximity to faults can impact the system lifetime, generated NPV and Heat In Place (HIP) recovery (Daniilidis et al., 2020a).

The development and exploitation of direct use, single doublet geothermal systems are subject to several uncertainties (Chen et al., 2015, 2019; Hoffmann et al., 2019; Schulte et al., 2020). The impact of uncertainties can be significant for the lifetime of a geothermal system (Daniilidis et al., 2021, 2020a, 2017a, 2016; Saeid et al., 2020).

* Corresponding author.
E-mail address: a.daniilidis@tudelft.nl (A. Daniilidis).

https://doi.org/10.1016/j.geothermics.2021.102041
Received 27 September 2020; Received in revised form 15 December 2020; Accepted 30 December 2020
Available online 20 January 2021

Table 1
The physical properties of the model components. The reservoir, over and underburden layers have a vertical permeability of an order of magnitude lower that the horizontal. The fault permeability is assigned to the normal to its plane, while along the fault plane the permeability is an order of magnitude higher. The fault permeability values are determined by the inputs from Table 2.

	Porosity (%)	Permeability (m^2)	Thermal conductivity (W/(m·K))	Specific heat capacity (J/(kg·K))	Density (kg/m^3)
max		4.93×10^{-13}			
mid	20	9.87×10^{-14}	2.9	970	2200
min		4.93×10^{-15}			
Fault	20	Parallel to fault plane: kFault×10 Normal to fault plane: kFault	2.9	970	2200
Overburden and basement	1	9.86×10^{-18}	2.2	1100	2400

Consequently, the energy produced from the system is affected and that can have an impact on the economic performance (Daniilidis et al., 2017a; Willems et al., 2017a). Previous research on interference between doublets has mostly considered single layer homogeneous reservoir conditions (Willems et al., 2017b). Recent research however, has shown the presence of a fault to significantly affect the system lifetime of a single doublet (Daniilidis et al., 2020a).

For single doublet systems, extensive sensitivity studies have been carried out on parameters such as fluid properties (Saeid et al., 2014), reservoir heterogeneity (Crooijmans et al., 2016), seasonal fluctuations in flow rate (Daniilidis et al., 2017b). The interference between doublets has been previously studied for homogeneous systems, including the arrangement of different well doublets identifying positive interferences for a checkerboard configuration (Willems et al., 2017b). Additionally, a doublet spacing that is equal to the well spacing between the individual doublets has been found beneficial for interference on both homogeneous (Willems et al., 2017b) and heterogeneous systems (Babaei and Nick, 2019). Nonetheless, studies on interference between doublets

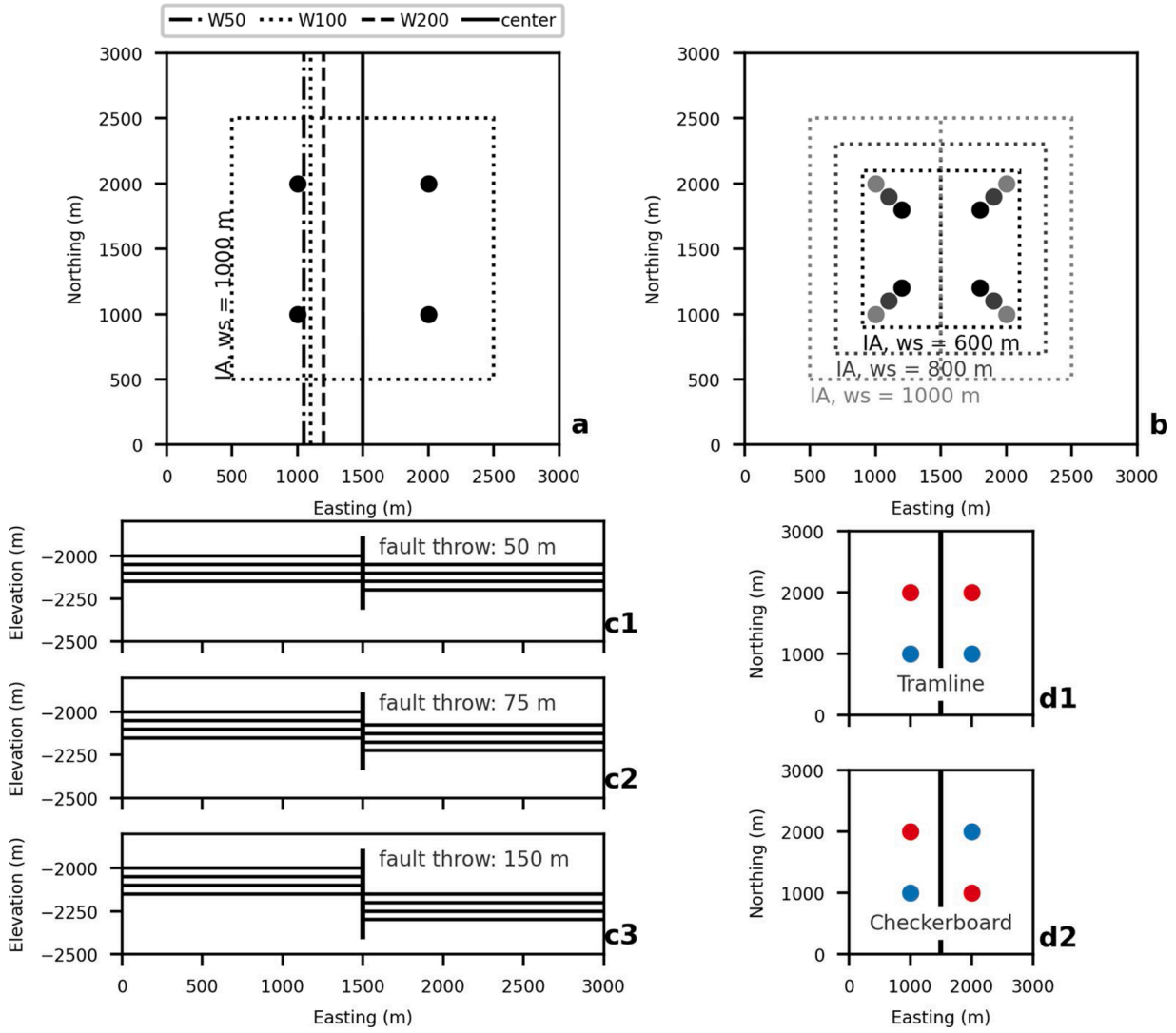

Fig. 1. Map view with the positioning of the fault (a) for a well spacing of 1000 m and the respective influence area of 2 km by 2 km; the well spacing options and the respective sizes of the influence area of two times the well spacing (b); vertical section of the model with showcasing a fault throw of 50 m (c1), 75 m (c2) and 150 m (c3) with the east block always displaced; tramline (d1) and checkerboard (d2) well configurations. A full list of the parameters used in the model is provided in Table 2.

across a fault have not yet been conducted.

As direct use geothermal systems transition towards multiple doublets by a single operator (Daniilidis et al., 2020b; Willems and Nick, 2019), the interference between adjacent doublets becomes more important. Field development decisions are made at early stages, where uncertainties remain high and system behaviour is not fully understood. It is pertinent to be able to assess the impact of faults as their presence might not always be known prior to development due to, for example, sub-seismic imaging resolution, 2D seismic data availability or the absence of seismic data altogether (Alcalde et al., 2017; Botter et al., 2014; Libak et al., 2017; Malz et al., 2015; Patel et al., 2008; Wang et al., 2018). Synthetic, representative models can aid in quantifying the interplay between these uncertainties. Such models can be easily parametrizable and computationally efficient allowing the simulation of a multitude of realizations that would require unrealistically long computation time at full scale.

The impact of large faults on the interference between adjacent doublet systems, in terms of the evolution of the thermal breakthrough and consequently on the system lifetime, generated economic value and HIP recovery is not currently explored. In this work we present a coupled, Thermal-Hydraulic (TH) model using the Finite Element Method (FEM), that profiles a sedimentary aquifer between an impermeable overburden and basement in synthetic, representative models. A full factorial study is carried out for two neighbouring doublets separated by a single fault. The study includes an extensive sensitivity of the fault throw, the fault permeability, the fault distance to the doublets, the well configuration, the well spacing, the flow rate, the reservoir depth and the sequence of the reservoir layers. A total of 5184 3D reservoir simulations are performed. The impact of subsurface uncertainty and operational choices on the system lifetime, produced cumulative energy, HIP recovery, economic output and Influence Area (IA) boundary temperature with respect to the wells production temperature is examined separately for each doublet, and also on the combination of both doublets.

2. Methods

The aim of the study is to identify factors that can affect the system lifetime, the economic performance and the HIP recovery of a geothermal system consisting of a single doublet within a faulted block. A number of different parameters are considered, in order to have a systematic overview of the interference across a fault. Design parameters such as well spacing and positioning and the fault distance to the doublets are considered. Flow properties of reservoir layers and the fault generate a range of reservoir architectures. Combining the design with the physical parameters enables capturing a multitude of juxtapositions in terms of possible fluid flow paths and sources/sinks of flow. The flow rate effect showcases how the system behaves at different intensities of exploitation. To show how all these effects interact, a full factorial design is performed comprising 5184 unique 3D reservoir simulations.

2.1. Design and inputs

The reservoir is comprised of three layers, each 50 m thick. These dimensions are meant to capture an abstraction of reservoirs considered as geothermal targets in sedimentary basins. The reservoir is confined between overburden and basement layers that exhibit very low porosity and permeability (Table 1), equivalent to impermeable rocks. The inclusion of an overburden and basement layer in the model is important as their thermal properties can have a significant effect on the produced energy (Daniilidis and Herber, 2017), and the thermal recharge can affect the system lifetime (Saeid and Barends, 2009). The confining layers have a thickness of at least 250 m to ensure sufficient thermal recharge over the simulation duration of 100 years.

The model includes two doublets separated by a fault. Both doublets are produced using the same rates as the geological context is the same and it is reasonable to expect comparable flow properties on both sides of the fault. The model domain is 3000 m by 3000 m while the spacing of the wells is varied between 600 m and 1000 m. The wells of each doublet are parallel to the fault which is aligned along the N–S axis; one doublet is positioned in the western part and one in the eastern part of the domain. The analysis considers the options that each block is developed by an individual developer (west and east) or by a single developer. In the first case each doublet has an individual analysis of production temperature and NPV, while in the latter case the mean temperature of the two doublets is considered and the NPV is computed accordingly.

Table 2
The input parameters considered in the analysis. All parameter combinations are considered in an experimental design that results in a dataset of 5184 3D reservoir simulations.

Parameter	
Fault Throw (m)	0, 50, 75, 150
Fault Permeability (m^2)	Sealing (9.86×10^{-18}), Transparent (4.93×10^{-13}), Conduit (9.86×10^{-13})
Fault distance (m)	W50, W100, W200, centre
Well configuration	Tram, Checkerboard
Well Spacing (m)	1000, 800, 600
Flow rate (m^3/h)	100, 250, 400
Top reservoir depth (m)	2000, 2500
Reservoir architecture (top to bottom)	min/mid/max, max/min/mid, min/max/mid

The fault plane itself has a thickness of 10 m, is vertical and extends throughout the whole length of the domain. The top of the reservoir remains constant for the west part (footwall) and is positioned at depths of 2 km and 2.5 km. The east part is offset by the fault throw (hanging wall). The fault throw considers only having a discontinuous surface but no offset (0 m throw), bringing two consecutive reservoir layers aligned across the fault surface (50 m throw), having an overlap between two layers on each side of the fault (75 m throw) and having a complete disconnection of the reservoir layers across the fault surface (150 m throw) (Fig. 1c). The fault position is varied at distances of 50 m (W50), 100 m (W100) and 200 m (W200) from the west doublet (Fig. 1a). When the fault is positioned at the centre between the two doublets, its distance to both doublets is a function of the well spacing used.

An IA is assigned with dimensions of the well spacing by two times the well spacing, as shown in Figure 1a&b. The dimensions of the IA are according to the considerations of the production license boundary in the Netherlands (TNO-AGE, 2014). Since the doublet spacing (along the easting) is always equal to the well spacing (along the northing) the combined influence area is a square (Fig. 1b). It should be noted that regardless of the fault position, the IA for each doublet is only a function of the well spacing (Fig. 1b).

The properties of the different model layers are listed in Table 1. The reservoir architecture is represented by alternating the sequence of the three reservoir layers and their respective flow properties. The reservoir layers exhibit the same porosity but their permeability takes one of the discrete values: max ($4.93 \times 10^{-13}\ m^2$), mid ($9.87 \times 10^{-13}\ m^2$) and min ($4.93 \times 10^{-15}\ m^2$). Reservoir permeability is isotropic on the horizontal plane, while the vertical permeability is an order of magnitude lower.

The fault permeability is isotropic along the fault plane (model y-axis/northing and elevation axes), while the permeability of the normal to the fault plane (model x-axis/easting) is an order of magnitude lower (Table 2 and Table 1), following observations from previous research (Faulkner and Rutter, 2001). Fault permeability takes three values: i) sealing, which is three orders of magnitude lower than the min layer of the reservoir and the same as the overburden and basement confining layers, ii) transparent, which is the same as the max reservoir layer and can be seen as only examining the impact of fault displacement and iii) conduit, which is two times higher than the max reservoir layer. The fault and reservoir layers have the same values of thermal conductivity and specific heat capacity. Porosity and permeability is the same for

Table 3
Inputs used in the economic calculations.

Load factor (%)	Heat price (€/MWh)	Pump cost (k€)	Pump lifetime (yrs)	Pump efficiency (%)	OpEx % of CapEx (%)	Annual Discount rate (%)	Electricity price (€/MWh)
90	60	500	5	60	5	7	100

overburden and basement layers (1 % and 9.86×10^{-18} m^2 respectively).

The well diameter is 21.59 cm (8.5″) for the low flow rate case of 100 m^3/h and 25.4 cm (10″) for the high flow rate case of 400 m^3/h. Table 3 summarizes the input used for the NPV calculations.

2.2. Reservoir model

A coupled Thermal-Hydraulic (TH) model is built in COMSOL Multiphysics (version 5.3a, build: 275). The simulator is selected due to its ability to accurately model all relevant physics processes, its flexibility in defining and adjusting the system geometry and controlling the mesh quality using a single software. Simulators that are specifically developed for subsurface fluid flow might yield shorter simulation time. However, for the scope of our studies the utility of the chosen simulator was deemed valuable, together with its flexibility in utilizing multicore systems for embarrassingly parallel problems (i.e. that benefit linearly with the number of available computing resources).

2.2.1. Initial conditions

The initial reservoir temperature is a function of depth and it is computed according to:

$$\mathrm{T} = T_{ref} - T_{grad} z \tag{1}$$

where T_{ref} is the reference temperature (°C) at surface conditions (taken here as 10 °C) and T_{grad} is the temperature gradient (taken here as 31 °C/km according to (Bonté et al., 2012)).

Initial pressure in the reservoir is a function of depth and is computed according to:

$$\mathrm{P} = p_{ref} - p_{grad} z \tag{2}$$

where p_{ref} is the reference pressure (MPa) at surface conditions (taken here as 0.1 MPa), p_{grad} is the pressure gradient (considered hydrostatic) and z is depth (m).

2.2.2. Governing equations

The Energy Balance describes the heat transfer in the model as follows:

$$\rho C \frac{\partial T}{\partial t} + \rho_f c_f \mathrm{q} \nabla T - \nabla.(\lambda \nabla T) = 0 \tag{3}$$

in which T (K) is the temperature, ρ the mass density (kg/m^3), c (J/(kg K)) the specific heat capacity, λ (W/(m K)) the thermal conductivity, q (m/s) the Darcy velocity and suffixes $_{\mathrm{f}}$ and $_{\mathrm{s}}$ refer to the fluid and the solid matrix respectively. The thermal conductivity and volumetric heat capacity of the system is computed based on the respective fluid and rock values separately according to:

$$\lambda = (1 - \varphi)\lambda_{\mathrm{s}} + \varphi \lambda_{\mathrm{f}} \tag{4}$$

and

$$\rho C = (1 - \varphi)\, \rho_s c_s + \varphi \rho_f c^f \tag{5}$$

in which φ is rock porosity. The pressure field is computed based on the continuity equation according to:

$$\varphi \frac{\partial \rho_{\mathrm{f}}}{\partial \mathrm{t}} + \nabla.\left(\rho_{\mathrm{f}}\, \mathrm{q}\right) = 0 \tag{6}$$

where the flux q (m/s) is defined by Darcy's law:

$$\mathrm{q} = -\frac{\mathrm{k}}{\mu}\left(\nabla \mathrm{P} - \rho_{\mathrm{f}} \mathrm{g} \nabla \mathrm{z}\right) \tag{7}$$

in which k is the intrinsic porous medium permeability (m^2), μ the dynamic viscosity of the fluid (Pa·s), g the acceleration of gravity (m/s^2), P the hydraulic pressure (Pa) and z is the depth (m). Fluid flow and energy balance are fully coupled in the model for the reservoir, wells, fault, overburden and underburden domains. Gravity effects are also considered throughout.

The fluid density (kg/m^3) and viscosity ($Pa{\cdot}s$) are a function of temperature according to:

$$\rho_f = 838.466135 + 1.40050603\mathrm{T} - 0.0030112376\mathrm{T}^2 + 3.71822313 \times 10^{-7}\mathrm{T}^3 \tag{8}$$

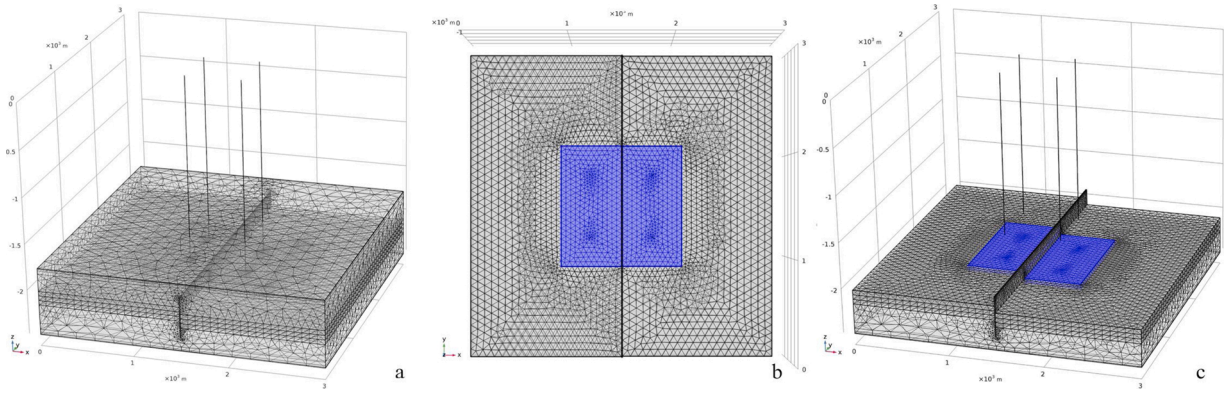

Fig. 2. Angled view of the meshed reservoir model (a), shown here for a well spacing of 600 m. The influence area with a size of two times the well spacing on the long side and one time the well spacing on the short side is highlighted (b), view of the higher mesh resolution around the wells and inside the influence area, with the overburdern removed (c). The number of elements ranges from 179k to 321k depending on the geometry configuration.

$$\mu = 1.3799566804 - 0.0212240191511T + 1.3604562827 \times 10^{-4}T^2 - 4.6454090319 \times 10^{-7}T^3 + 8.9042735735 \times 10^{-10}T^4 - 9.0790692686 \times 10^{-13}T^5 + 3.8457331488 \times 10^{-16}T^6 \quad (9)$$

The discrepancy between the pressure solution from eq 2 and eq 8 is resolved within the first timesteps of the simulation.

2.2.3. Mesh

The consideration for the mesh was to enable high enough result accuracy while maintaining a reasonable run time for the simulation ensemble. The model is meshed using a higher number of tetrahedral elements inside the reservoir layers, where flow is taking place (Fig. 2a). An additional refinement is performed around the wells where the higher flow velocities occur (Fig. 2b). Moreover, within the subdomain area (see Fig. 2) a further refinement is applied ensuring a minimum of three vertical cells per reservoir layer. The minimum element size inside the reservoir domain is 5 m and the maximum is 70 m. A mesh analysis study was performed to confirm that the chosen mesh sizes provide sufficient accuracy of model results.

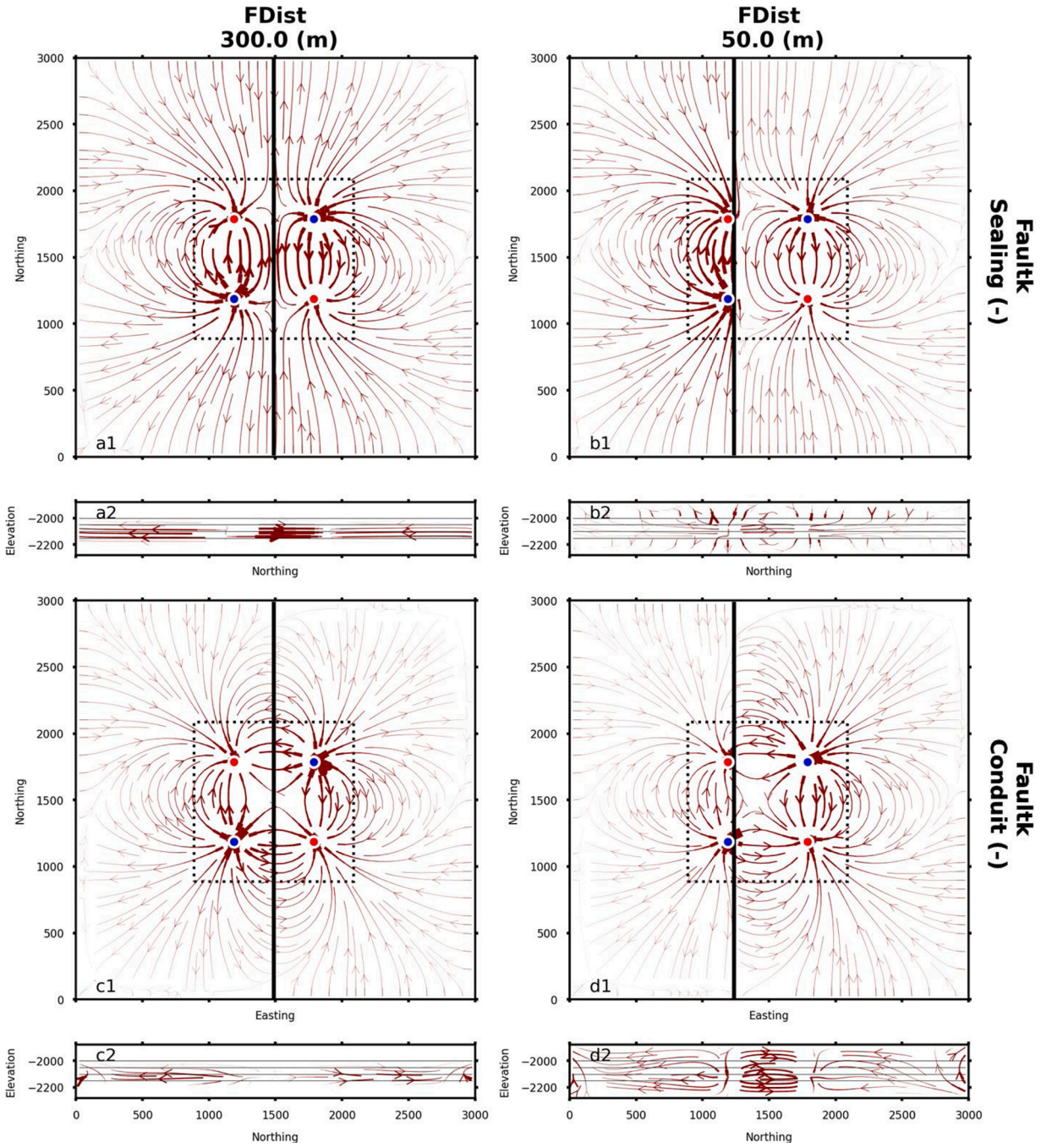

Fig. 3. Horizontal section of the flow field at the base of the reservoir for a fault distance of 300 m (a1) and 50 m (a2) with a sealing fault and conduit fault respectively (c1 and d1) and their respective fault plane plots (a2,b2, c2, d2). Data shown use a checkerboard well configuration, a well spacing of 600 m, a fault throw of 0 m, a reservoir architecture of mid/min/max, a west reservoir top depth at 2 km and a flowrate of 400 m^3/h. The dotted lines delineate the extent of the IA as defined in Fig. 1. The respective flow field for a tramline configuration can be found in Fig. 24.

2.3. Well model

A simple well model is implemented in order to accommodate a flow rate control on the wells. The well rate is partitioned to each layer based on the ratio of the *kh* (permeability-thickness) of each layer to the *kh* of the whole reservoir interval as formulated in (Jalali et al., 2016):

$$q_i = \left(k_i h_i \Big/ \sum_{1}^{m} k_i h_i \right) q_{total} \tag{10}$$

in which k_i (m^2) and h_i (m) are the permeability and thickness of layer i respectively, m is the total number of layers and q_i and q_{total} are the layer i flow rate and the total flow rate respectively. The reported well temperature and pressure in the results section is the respective average value over the height of the reservoir section. The wells are governed by coupled fluid flow and heart transfer (section 2.2.2 Governing equations). Pressure and temperature along the wellbore to the surface is not considered since the focus is on the reservoir performance. However, previous studies have shown the temperature effects along the wellbore caused by heat exchange with the surrounding rock to be negligible (less than 1 °C) for simulation periods longer than 5 days (Saeid et al., 2015).

2.4. Initial and boundary conditions

A geothermal gradient of 31 °C/km (Bonté et al., 2012) and a hydrostatic pressure gradient of 10 MPa/km are applied as initial conditions to the whole model domain. A pressure boundary condition is applied to the sides of the model, equal to the initial values calculated through the hydrostatic pressure gradient.

The model boundary conditions for flow include no flow boundaries on the top and bottom surfaces of the model, while all side boundaries are open to flow. Temperature boundaries include a fixed temperature at the top and bottom of the model according to the initial conditions, while all side boundaries are open to heat transfer.

2.5. Heat in place (HIP)

The calculation of the Heat In Place (HIP) is carried out according to:

$$HIP = \int_{0}^{V_{subdomain}} \left(\left(\rho_f c_f \varphi + \rho_s c_s (1-\varphi) \right) (T - T_{inj}) dV \right) \tag{11}$$

The HIP is calculated before any production takes place. The lower bound of the temperature difference is taken as T_{inj} as that is the lowest threshold that can effectively be recovered from the system (Garg and Combs, 2015). The HIP is calculated only inside the reservoir volume outlined by the IA extent (Fig. 2).

2.6. System lifetime and NPV

The system lifetime is reached at time t, when the condition for the temperature (°C) of the hot water from the production well is 95 % of the initial production temperature (t = 0)

$$T_{prod_t} \leq 0.95 T_{prod_{t=0}} \tag{12}$$

is met. This condition is quite sensitive and is meant to identify the moment at which a slight change in the production temperature is measured. It therefore can be considered as a worst-case scenario for lifetime, bearing in mind that a temperature drop of less than 10 °C may still not compromise the operation of the geothermal system. Nonetheless, such a normalized definition of the production temperature enables cross-comparison between the results. The produced power used for the calculation of income is computed according to:

$$P_{well} = Q \rho_f \, c_f \, \Delta T \tag{13}$$

in which Q is the flow rate (m^3/s) and ΔT is the temperature difference between producer and injector wells (°C). The respective producer and injector well temperature is the average temperature for the well over the reservoir interval. The required pump power only considers the pressure drop in the reservoir:

$$P_{pump} = \frac{Q \Delta P}{\eta} \tag{14}$$

where ΔP is the pressure difference between the wells and η is the pump efficiency. The respective producer and injector well pressure is the average pressure for the well over the reservoir interval. The overall system power is then calculated as:

$$P_{system} = P_{well} - P_{pump} \tag{15}$$

The cost of the wells in € is computed according to (TNO, 2018):

$$C_{well} = 375000 + 1150Z + 0.3Z^2 \tag{16}$$

where Z is the measured depth. For the high flow rate cases that utilize a larger production diameter, the above calculated well cost is increased

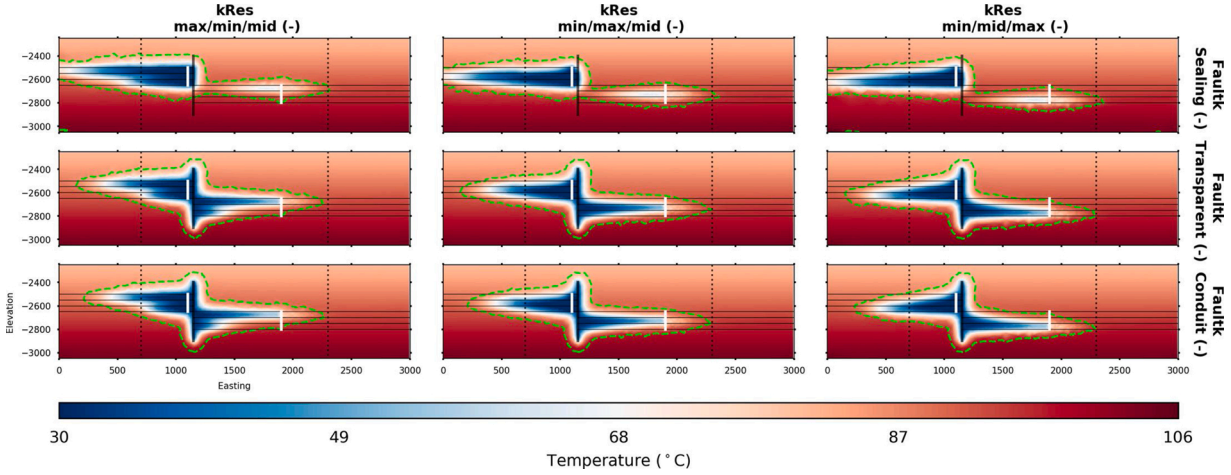

Fig. 4. Reservoir temperature on a vertical section along the South set of wells for the different reservoir architectures and fault permeability values, after 50 years of production. Data shown use a checkerboard well configuration, a well spacing of 800 m, the fault positioned 50 m away from the west injector, a fault throw of 150 m, a west reservoir top depth at 2.5 km and a flowrate of 400 m^3/h. The dotted lines delineate the extent of the IA as defined in Fig. 1, while the lime coloured line outlines a 1 °C temperature drop.

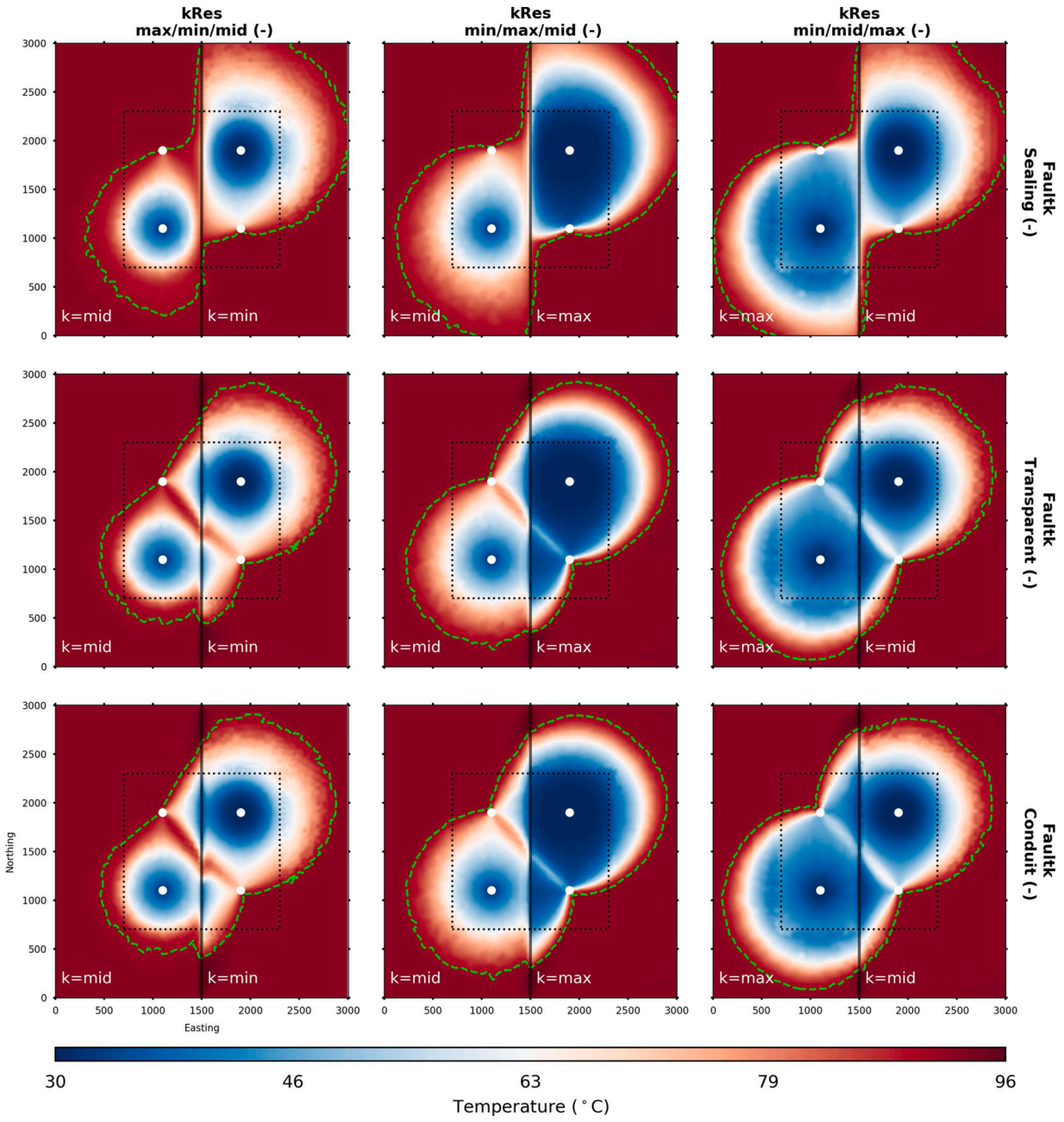

Fig. 5. Horizontal section of the reservoir at the base of the west reservoir layers (depth of 2650 m), for the different reservoir architecture and fault permeability values after 50 years of production. Data shown use a checkerboard well configuration, a well spacing of 800 m, a flow rate of 400 m^3/h, a fault positioned at the centre, a fault throw of 75 m and a west reservoir top depth at 2.5 km. The dotted lines delineate the extent of the IA as defined in Fig. 1, while the lime coloured line outlines a 1 °C temperature drop.

by 25 %. The NPV is then calculated as:

$$NPV = \sum_{t=0}^{n} \frac{CF_t}{(1+r)^t} \tag{17}$$

Where *CF* is the cashflow, *r* the discount rate, *n* is the project years and *t*. the time intervals. The cumulative produced power generated income is based on the heat price, while the pump power costs are computed based on the electricity price (see Table 3). The NPV and HIP recovery data are selected at the point in time where the system lifetime condition is reached.

Three different options are consider when computing the NPV: a) each doublet is operated by an individual developer (east, west), b) both doublets are operated by a single developer and the production temperature is the mean of the both doublets and c) both doublets are operated by a single developer but are kept separate, so each doublet has its own lifetime and NPV.

3. Results

3.1. Flow field

Fault permeability and fault proximity to the west doublet significantly affect the flow field (Fig. 3). The flow pattern inside the reservoir is stronger in between the wells of each doublet and becomes weaker closer to the domain boundaries for all cases. A conduit fault allows flow perpendicular to the fault plane (Fig. 3c & d), connecting the two fault sides. For a conduit flow and a fault distance of 50 m from the west

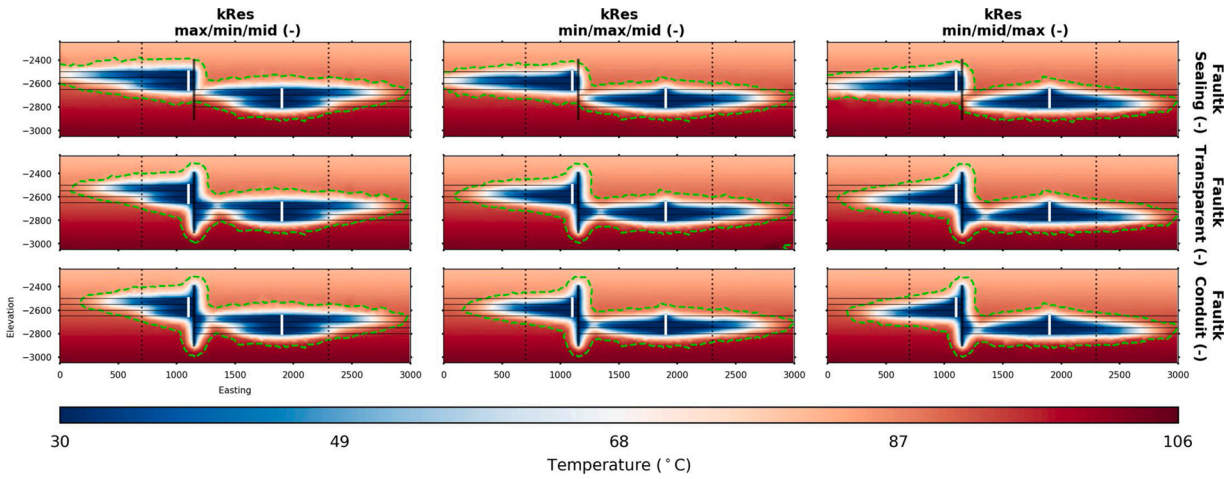

Fig. 6. Reservoir temperature on a vertical section along the South set of wells for the different reservoir architectures and fault permeability values, after 50 years of production. Data shown use a tramline well configuration, a well spacing of 800 m, the fault positioned 50 m away from the west injector, a fault throw of 150 m, a west reservoir top depth at 2.5 km and a flowrate of 400 m^3/h. The dotted lines delineate the extent of the IA as defined in Fig. 1, while the lime coloured line outlines a 1 °C temperature drop.

doublet the flow pattern is stronger in the area between the two wells, but also extends towards the edges of the domain. For a sealing fault (Fig. 3a and b) a sharp boundary in the direction of the flow field along the fault plane is observed (Fig. 3a1 & b1). With the fault at the centre between the two wells (a2 and c2), flow inside the fault plane is limited to the reservoir depth and is stronger at the reservoir depth corresponding to the highest permeability. Close proximity to the west doublet results in flow over the whole height of the fault (b2, d2).

3.2. Cold water front

3.2.1. Checkerboard well configuration

An increased interference between the two doublets is observed as the fault permeability is increasing for the checkerboard well configuration (Fig. 4). For a sealing fault and regardless of the reservoir architecture we observe limited temperature interreference between the west and east block, limited only to conductive heat transport since there is no hydraulic connection between the blocks (Fig. 4, top row). With increasing fault permeability, the two blocks are hydraulically connected and the cold plume from the western block connects to the producer well from the east block (Fig. 4, middle row). Additionally, the area around the fault also exhibits a temperature drop since cold water now circulates through the fault surface. The propagation of the cold front is more prominent in the high permeability reservoir layer. A conduit fault does not show significant differences in the shape of the cold front compared to the transparent fault (Fig. 4, bottom row). The 1 °C temperature drop always exceeds the influence area boundary, but the sealing fault amplifies the distance of the temperature drop with respect to injection well of the west block.

The map view of the base of the west reservoir for the well configuration shown in Fig. 4 shows the differences in the lateral extent of the cold water plume (Fig. 5). When the fault is sealing the interaction across the two blocks is limited to the flow of cold water along the fault surface on either side on the respective production well part and only to conduction effects on each side on the respective production well part (Fig. 5, top row). The shape and size of the cold plume on each side is proportional to the respective reservoir layer permeability (see also Fig. 4), with larger sizes and sharply defined edges being the result of higher layers permeability. For a transparent fault permeability (Fig. 5, middle row) the two blocks are hydraulically connected and cold water from both injectors connects to the producer of the other block and the lateral extent of each cold plume is reduced compared to the sealing fault. For the lower permeability layers, the cold water plume extends further across the fault as it is diverted along the fault plane. The permeability contrast encountered across the fault dictates if the plume is narrowed (moving from higher to lower permeability) or widened (moving from lower to higher permeability). The extent of the cold water plume with respect to the IA is further discussed in section 3.6.

3.2.2. Tramline configuration

Similar to the checkerboard configuration, the tramline configuration exhibits wider lateral extents in the west block of the cold front and 1 °C temperature drop when the fault is sealing (Fig. 6, top row). With a transparent and conduit fault (Fig. 6, middle and bottom row respectively) interference increases and lower temperature is also observed along the fault direction. However, no distinction can be observed between the two fault permeabilities or the reservoir architectures in terms of the interferences between the two blocks.

For the tramline well configuration with the injector wells being in the south part of both the east and west block the cold plume does not extend beyond the producer wells to the north of the domain when the fault is sealing (Fig. 7, top row). With a fault transparent permeability the cold water flows through the fault plane, creating a shortcut between the injection and production wells (Fig. 7, middle row) and also extending the 1 °C temperature drop to the south along the fault plane. However, the latter extents of the cold plume are not significantly different compared to the sealing fault. On the north part of the domain and around the fault a slight increase in temperature can be observed which could be the result of a forced convection cell on the fault plane. No significant differences are observed between the transparent and conduit fault (Fig. 7, bottom row).

3.2.3. Flow rate and fault position

With increasing flow rate, the interference between the east and west block increases accordingly (Fig. 8, top row). With a flow rate of 100 m^3/h the 1 °C temperature drop of the two blocks only starts to connect when the fault is 200 m or more away from the west injector well. With the fault positioned in the middle between the two blocks only the lower part of the fault reaches a 1 °C temperature drop, while the top part is not influenced by the cold plume. At 250 m^3/h the 1 °C temperature drop is already present at both the top and base of the fault and it is connected between the two blocks regardless of the fault position (Fig. 8, middle column). With the exception of the fault being in the centre between the two blocks, the connection of the west and east parts is centred around the high permeable layer. With the highest rate of 400 m^3/h the connection between the two blocks is slightly more

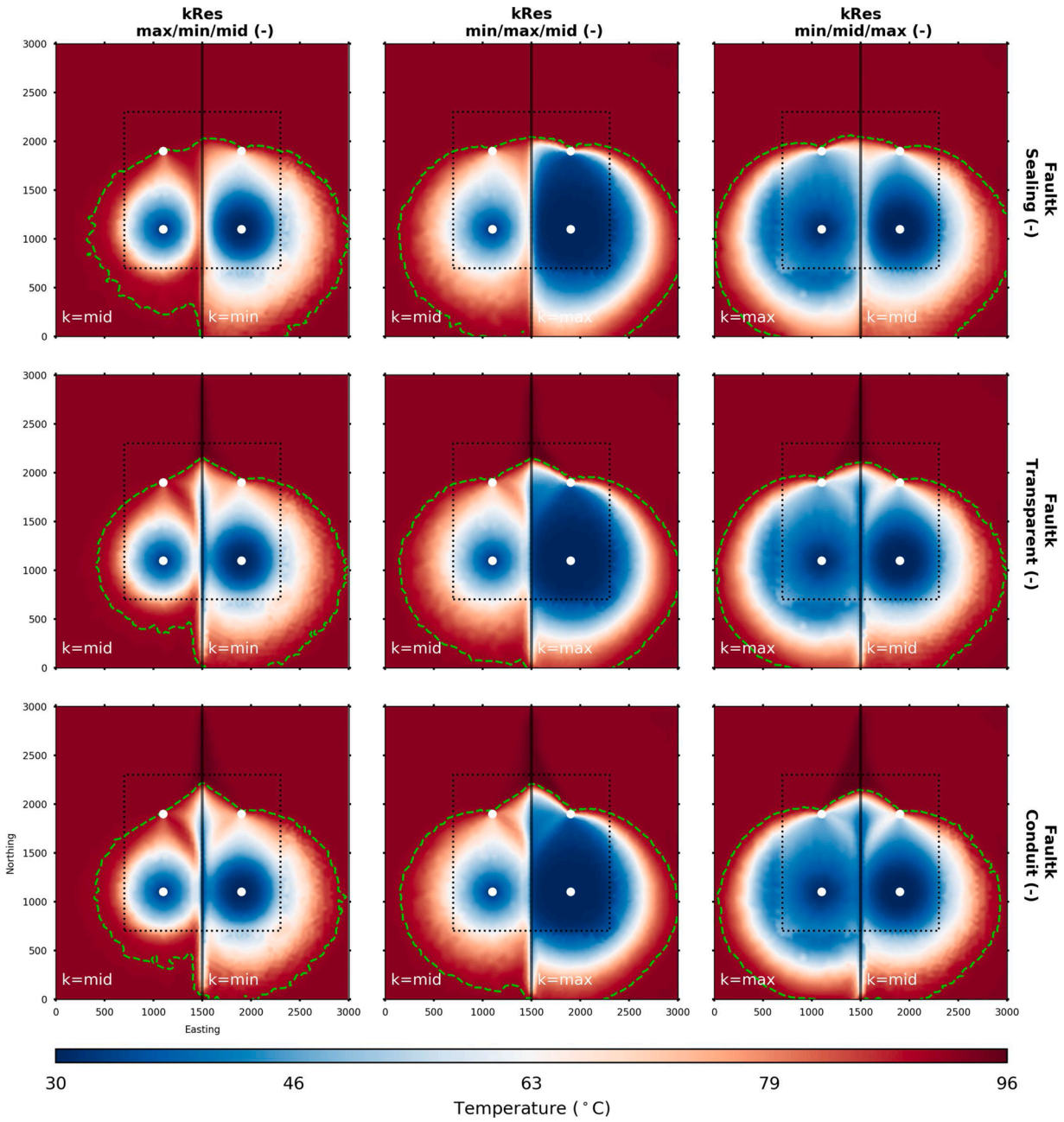

Fig. 7. Horizontal section of the reservoir at the base of the west reservoir layers (depth of 2650 m), for the different reservoir architecture and fault permeability values after 50 years of production. Data shown use a tramline well configuration, a well spacing of 800 m, a flow rate of 400 m^3/h, a fault positioned at the centre, a fault throw of 75 m and a west reservoir top depth at 2.5 km. The dotted lines delineate the extent of the IA as defined in Fig. 1, while the lime coloured line outlines a 1 °C temperature drop.

pronounced, even though a localization around the most permeably reservoir layers is still present (Fig. 8, right column).

For the high flow rate of 400 m^3/h the system lifetime, calculated from the mean temperature of both production wells on either side of the fault, assuming a single operation on both sides is shown in Fig. 9. When the fault is 50 m away from the west doublet (top row) the system lifetime decreases as the fault permeability increases from sealing, to transparent to conduit respectively. This is due to a hydraulic shortcut that allows the cold plume to reach the west producer via the fault, as the fault permeability increases, thus reducing the system lifetime. Along each individual column, with the fault position moving towards the centre of the block, the system lifetime is increasing respectively. When the fault is positioned in the middle of the block, a conduit fault exhibits the longest lifetime, since now the cold plume that enters the fault plane is diverted away from both producers, thus extending system lifetime. At a distance of 200 m away from the west doublet, a transparent of conduit fault permeability leads to longer lifetimes compared to a sealing fault. Therefore, the position of the fault becomes important in defining if the fault connects the wells of a single doublet, creating a shortcut, or if it acts as a diverting path that extends lifetime. For all data shown in Fig. 9 the 1 °C drop extends beyond the boundaries of the IA laterally, an aspect further discussed in section Influence area.

3.3. Fault distance, throw and reservoir architecture effect on system lifetime

The interference of the fault with geothermal operations on either side increases with proximity to the fault, but it varies greatly depending

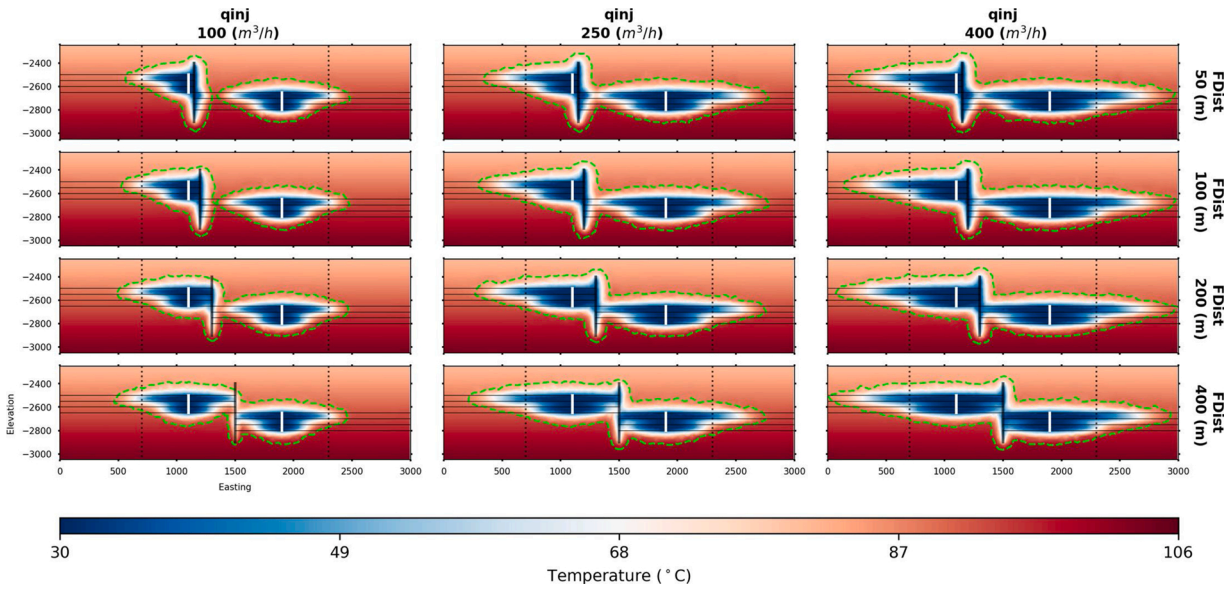

Fig. 8. Reservoir temperature on a vertical section along the South set of wells for all the flow rates and fault distance values, after 50 years of production. Data shown use a tramline well configuration, a well spacing of 800 m, a fault throw of 150 m, a west reservoir top depth at 2.5 km and a reservoir architecture of max/min/mid. The dotted lines delineate the extent of the IA as defined in Fig. 1, while the lime coloured line outlines a 1 °C temperature drop.

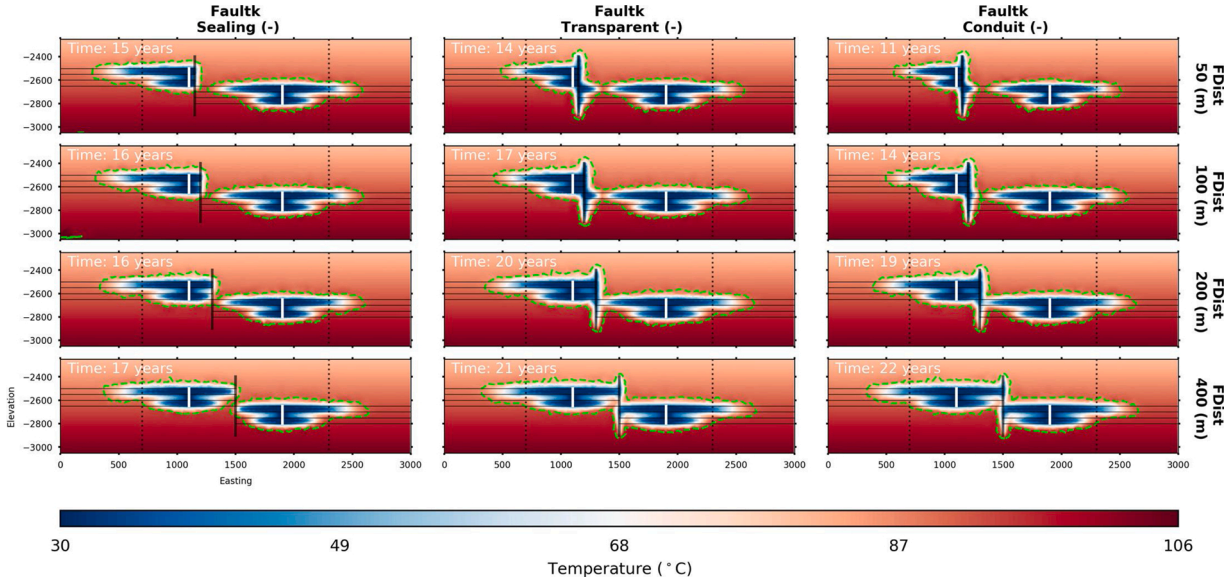

Fig. 9. Reservoir temperature on a vertical section along the South set of wells for all the fault permeability and fault distance values, at the time of thermal breakthrough (see eq. 12) of the mean production temperature of both wells (single developer - mean), denoted in white for each subplot. Data shown use a tramline well configuration, a well spacing of 800 m, a flow rate of 400 m^3/h, a fault throw of 150 m, a west reservoir top depth at 2.5 km and a reservoir architecture of max/min/mid. The dotted lines delineate the extent of the IA as defined in Fig. 1, while the lime coloured line outlines a 1 °C temperature drop.

on the hydraulic properties of the fault itself and on fault throw (Fig. 10). If the fault is sealed and prevents a hydraulic connection between the western and the eastern parts of the reservoir, the only major effect it has is the effective limitation of reservoir size, depending on the distance of the fault to the wells, with a corresponding effect on the lifetime. If the fault is in the centre between the two well doublets, both systems have identical lifetimes (Fig. 10, top row). Note that lifetimes are calculated for each side of the fault separately, assuming two independent operations on either side.

If the fault is not sealing, the fault throw has a clear effect on the expected lifetime. For a fault throw of 0 m, the lifetime on the eastern side is longer the closer the fault is to the western well doublet, with a correspondingly shorter lifetime on the western side. When the fault is in the centre, lifetime for both sides is identical, as the reservoir layer properties on both sides are identical and homogeneous. With a fault throw of 150 m, the difference in lifetime between the Eastern and Western sides is smaller than for no offset, but they are never identical, even when the fault is in the centre. There is also an obvious difference between a transparent and a fully permeable fault (Fig. 10 middle and bottom rows, respectively). In the transparent fault scenario, a fault throw of 150 m generally leads to a higher lifetime on both sides of the fault compared to fault throw of 0 m, while in the conduit fault scenario the reservoir architecture has a much greater influence on how much the fault throw affects the life time: the lifetimes on both sides are longest when the top layer is the most permeable of the stack (Fig. 10 middle column) and the shortest when the most permeable layer is in the middle

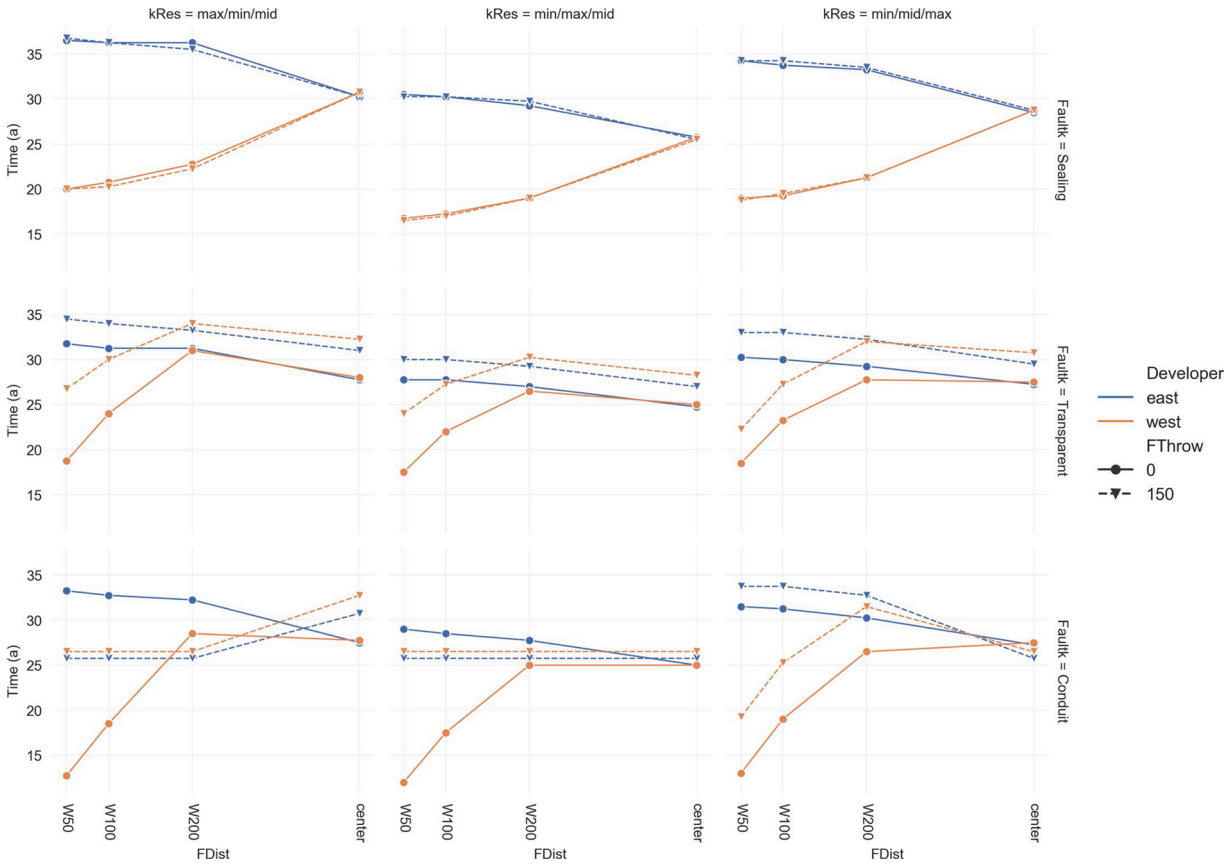

Fig. 10. System lifetime against fault position for all the reservoir architectures and fault permeability values, coloured by the east and west doublet individual developers, and marked for the different fault throw values. Data shown use a checkerboard well configuration, well spacing of 1000 m, a top west reservoir depth of 2.5 km and a production rate of 400m^3/h.

(Fig. 10, right column)

With a fault throw of 150 m, the difference between the Eastern and Western sides for both, the transparent and conduit fault scenarios, depends largely on the reservoir architecture. When the most permeable layer is at the bottom of the reservoir sequence (Fig. 10, left column), lifetime on the Eastern side is larger when the fault is closer to the Western well doublet, but moving the fault further towards the centre increases the lifetime on the Western side greatly. The differences for the two sides become much smaller and are even reversed when the fault is in the centre, such that the lifetime on the Western side is slightly longer than on the Eastern side. For the other reservoir architectures investigated here, with the most permeable layer in the middle or on top of the stack, lifetimes on both sides of the fault are similar, independent of the relative distance to the fault, with a slight advantage for the Western side. For the reservoir architecture with the most permeable layer at the bottom and the least permeably layer at the top (right column) a positive interference is observed with the fault 200 m away from the west doublet. This can be attributed to the conductive heat exchange between the two layers having a positive influence with respect to the convection heat transfer (see also Fig. 13). This influence is not as significant when the fault is closer and the west doublet starts exhibiting reduced system lifetime. When the top layer is the most permeable and the fault is in the centre, lifetime for both sides is higher than for a fault throw 0 m.

The spacing between production and injection well is also a major parameter influencing lifetime. For the minimum well spacing chosen in our study, the interference of the fault is minimal. A well spacing of 600 m on both sides of the fault leads to a relatively short lifetime of about 10 years, in all scenarios shown in Fig. 11. Note that lifetimes are calculated from the mean temperature of both production wells on either side of the fault, assuming a single operation on both sides. For larger well spacing, the interference of the fault becomes more evident. The reservoir architecture has a strong impact on how the fault proximity influences lifetime by controlling the juxtaposition of the layers across the fault. For the sealing fault, lifetimes increase as the fault moves away from the western wells towards the centre, for a well spacing of 800 m and 1000 m and the results are identical for both tramline and checkerboard well configurations.

For the non-sealing fault scenarios, the effect of well spacing depends also on the configuration of the wells, the tramline vs. the checkerboard configuration. The checkerboard configuration has been found favourable in terms of lifetime in geothermal systems without a fault separating the wells (Willems et al., 2017b). Our analysis shows that the checkerboard is only favourable when the fault is close to one well pair, while the tram line configuration clearly leads to longer lifetimes when the fault is in the centre. This effect is most pronounced for the largest well spacing. The well spacing of each doublet is the same as the distance between the two doublets at all times (see also Fig. 1b).

The distance from the fault at which the tramline leads to longer lifetimes compared to the checkerboard configuration depends also on the reservoir architecture. If the most permeable layer is on the top of the reservoir unit (Fig. 11, left column), the tram line configuration is more favourable, especially for a larger well spacing, even if the fault is relatively close to the western wells. In this scenario, the most permeable layer on the eastern side of the fault communicates with the medium permeable layer on the western side. If the most permeable layer is at the bottom of the stack (Fig. 11, right column), the tramline configuration is only favourable when the fault is close to the centre between the two well doublets.

In general, the lifetime of the system depends on the hydraulic connectivity across the fault. For the tramline configuration, lifetimes

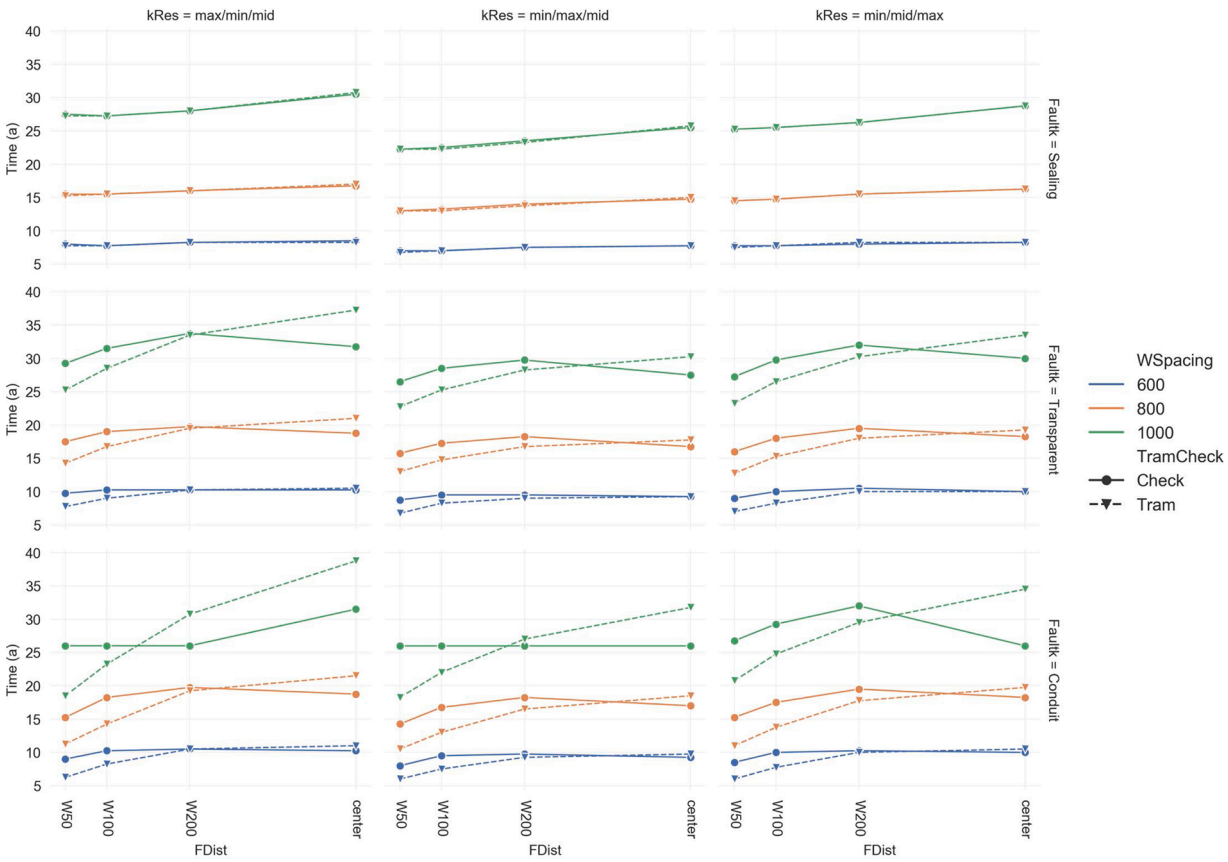

Fig. 11. System lifetime against fault position for a single developer (mean temperature of both production wells) for all the reservoir architectures and fault permeability values, coloured by the well spacing and marked for the different well configurations. Data shown use a fault throw of 150 m, top west reservoir depth of 2.5 km and a production rate of 400m^3/h.

are generally higher the better the hydraulic connection between the two sides is. It is therefore highest for the reservoir architecture with the most permeable layer on the top (Fig. 11, left column), which then connects with the medium permeable layer in the footwall (Fig. 1 c3). The lowest hydraulic connectivity is reached if the least permeable layer is on top of the reservoir unit, and the medium permeable layer at the bottom (Fig. 11, central column). This also leads to the overall lowest lifetimes with the tram line configuration. For the checker board, such a clear dependency is not obvious.

If the fault is fully permeable, its influence on reservoir performance strongly depends on the distance of the wells to the fault, but also on well spacing and injection rate (Fig. 12). Reservoir architecture does not play a major role, only the lifetime is slightly longer in most scenarios when the most permeable layer is on top. Generally, the effect of the fault distance is most pronounced if the well spacing is small and the flow rate is low or if the well spacing is large and the flow rate is fast. For the relatively large well spacing of 1000 m and flow rates of 100 m^3/h the effect of the fault distance becomes negligible, and also for the smallest well spacing of 600 m in combination with large flow rates, the effect is relatively small. This coupling of the effect of flow rate and well spacing also affects the influence of the well configuration. Generally, the lifetime of the system using a tramline configuration is much more strongly affected by fault distance than the checkerboard configuration. While the checkerboard configuration seems to be favourable for small fault distances, for larger fault distances the tram line configuration is better. This effect is most strongly observed for low flow rates when the well spacing is small, and only minor for the fastest flow rates of 400 m^3/h; in contrast, for the largest well spacing, well configuration has no effect for slow flow rates, while it has a strong effect at fast flow rates.

The change in system lifetime for a single developer with respect to the fault positioned at the centre shows a clear preference of the checkerboard configuration (Fig. 13). A tramline configuration always results in a reduction of system lifetime with respect to the fault positioned at the centre. For the high flow rate of 400 m^3/h this reduction can be more than 40 % when the fault is 50 m away from the west doublet (e.g. Fig. 13 left column, bottom row). Notably, an increase in system lifetime is observed for the reservoir architecture with the maximum producing layer on the bottom and the minimum producing layer on the top (right column). This increase is more significant for lower rates (100 and 250 m^3/h) up to a well spacing of 800 m. The larger well spacing of 1000 m combined with a checkerboard configuration shows and low and medium rates shows no negative lifetime effects when the fault is moving from the centre up to 50 m away from the west doublet. On the contrary, for a well spacing of 1000 m the highest positive interference occurs at a fault distance of 200 m for the highest flow rate of 400 m^3/h and results in a lifetime increase of more than 20 %.

3.4. Lifetime and NPV

The generated NPV is primarily dependent on the used rate and on a second level on the reservoir depth that results in an increasing production temperature and therefore energy production (Fig. 14). A flow rate increase of by a factor four between 100 m^3/h and 400 m^3/h results in a five-fold increase in NPV. For a rate of 100 m^3/h no significant NPV gains are observed for producing more than 5 TW h and therefore extending the system lifetime beyond 30 years does not yield any economic benefits despite the additional produced energy. Increasing the rate to 250 m^3/h a lifetime of more than 15 years already yields higher NPV compared to that produced with a rate of 100 m^3/h with any

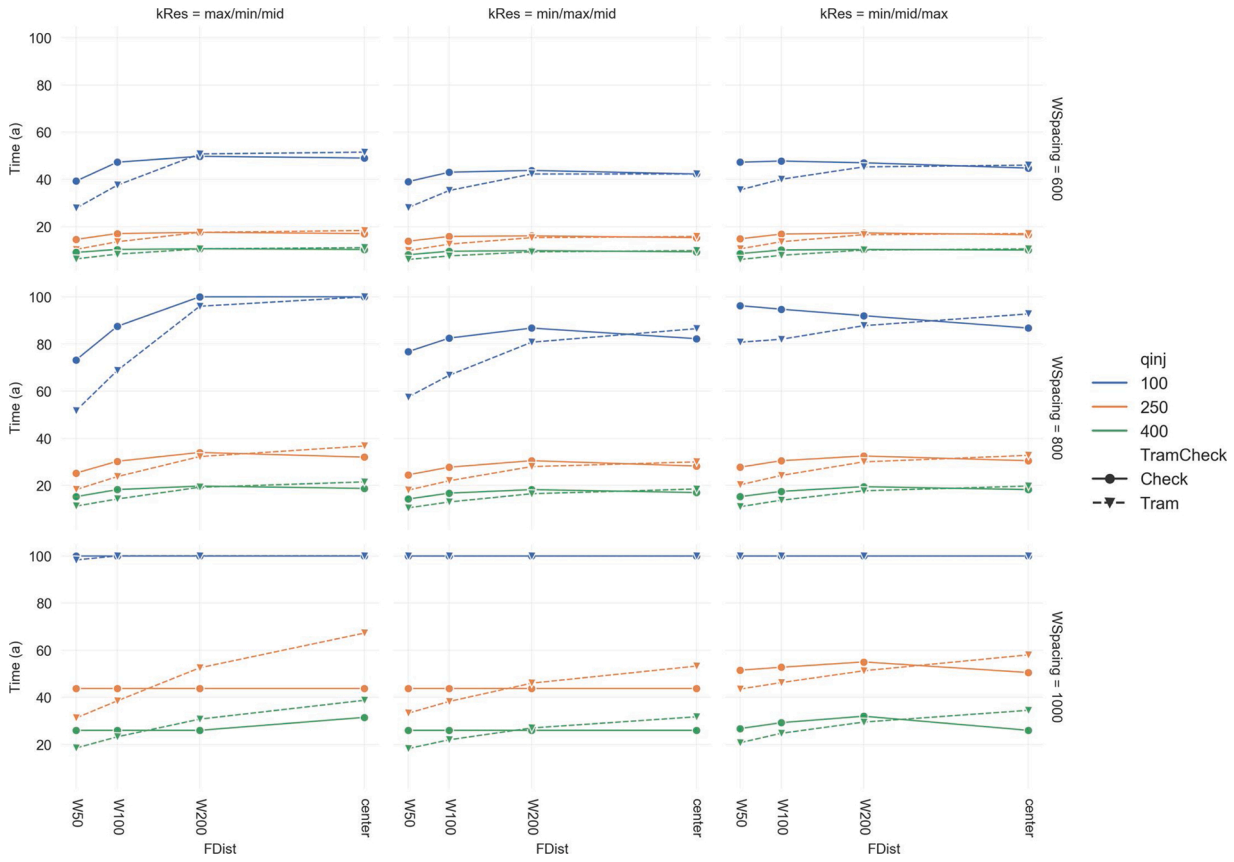

Fig. 12. System lifetime against fault position for a single developer (mean temperature of both production wells) for all the reservoir architectures and well spacing values, coloured by the production rate and marked for the different well configurations. Data shown use a conduit fault permeability, a fault throw of 150 m and a top west reservoir depth of 2.5 km. See supplementary information for a plot of the generated energy.

lifetime. Beyond the production of 12.5 TW h for the shallower (2 km) and 15 TW h for the deeper (2.5 km) reservoir depth no significant gains in terms of NPV can be seen. Further increasing the rate to 400 m^3/h shows that despite the shorter lifetime and lower amount of produced power, the shallower reservoir (2000 m) yields comparable NPV to the deeper reservoir produced with 250 m^3/h. The deeper reservoir (2.5 km) produces yet higher NPV for a comparable amount of generated power when produced at 400 m^3/h rates compared to the 250 m^3/h rates deep reservoir. Therefore, shorter lifetime is offset by the higher energy production of the higher rates resulting in comparable amounts of energy produced. The dataset for the higher rates does not show any sign of asymptotic behaviour suggesting that further increase of NPV can be achieved with prolonged system lifetime.

The fault position can have both positive and negative effects on the generated NPV (Fig. 15). A tramline configuration always leads to an NPV decrease as the fault moves closer to the west doublet. This decrease is more significant as flow rate is increasing. Contrary to this, a checkerboard configuration only reduces the generated NPV by less than 10 % in for the shorter well spacing and a distance of 50 m between the fault and the west doublet. The combination of well spacing and fault distance can even yield positive NPV effects, most prominently for a distance of 200 m and the larger well spacings of 800 m and 1000 m. These positive effects are larger when the minimum reservoir layer is at the top of the stack, favouring heat exchange across the two blocks with reduced convective losses.

3.4.1. *Single vs individual developers*

Shorter system lifetimes yield increasing NPV benefits when higher rates are used (see also Fig. 14) and the difference between the individual developers (west, east doublets) and the single developer (mean) increases with increasing rates (Fig. 16). For the low rates and for both considered depths the differences between the single developer (mean) are only attributed to the lifetimes of the individual doublets (west or east) respectively. No distinction can be made between a single developer (mean) and the single developer (separate) NPV. With a rate of 250 m^3/h and a depth of 200 m the individual developers (west & east) show again minor differences only attributed to the respective lifetime. The single developer (mean) results in both higher and lower NPV compared to the single developer (separate) case. This can be attributed to the cases where significant differences are present between the two individual doublets, as then the single developer (separate) would utilize the maximum lifetime for each system. When the lifetimes of both systems are close, the single developer (mean) results in higher NPV due to the higher revenues during the first years. At a depth of 2500 m the individual developers have reached their asymptotic NPV value while the single developer (mean) still increases slightly with longer system lifetime. With the highest rate of 400 m^3/h we see the difference between the single the individual developers further increasing with system lifetime and this effect is further amplified with a depth of 2500 m for the top of the reservoir. At the same time the discrepancy between the single developer and the single developer (separate) also increases with higher rates and deeper systems.

The generated NPV with respect to the fault positioning for the west, east or a single developer shows that a checkerboard configuration is increasingly beneficial for the west and single developer as the fault is closer to the west doublet (Fig. 17). When a flow rate of 100 m^3/h is used difference for all three development options are negligible. Increasing the production rate to 250 m^3/h leads to differences of circa 20 M€ for the west and circa 25M€ for the single developer when the fault position is closer than 200 m from the west doublet. The east developer is not

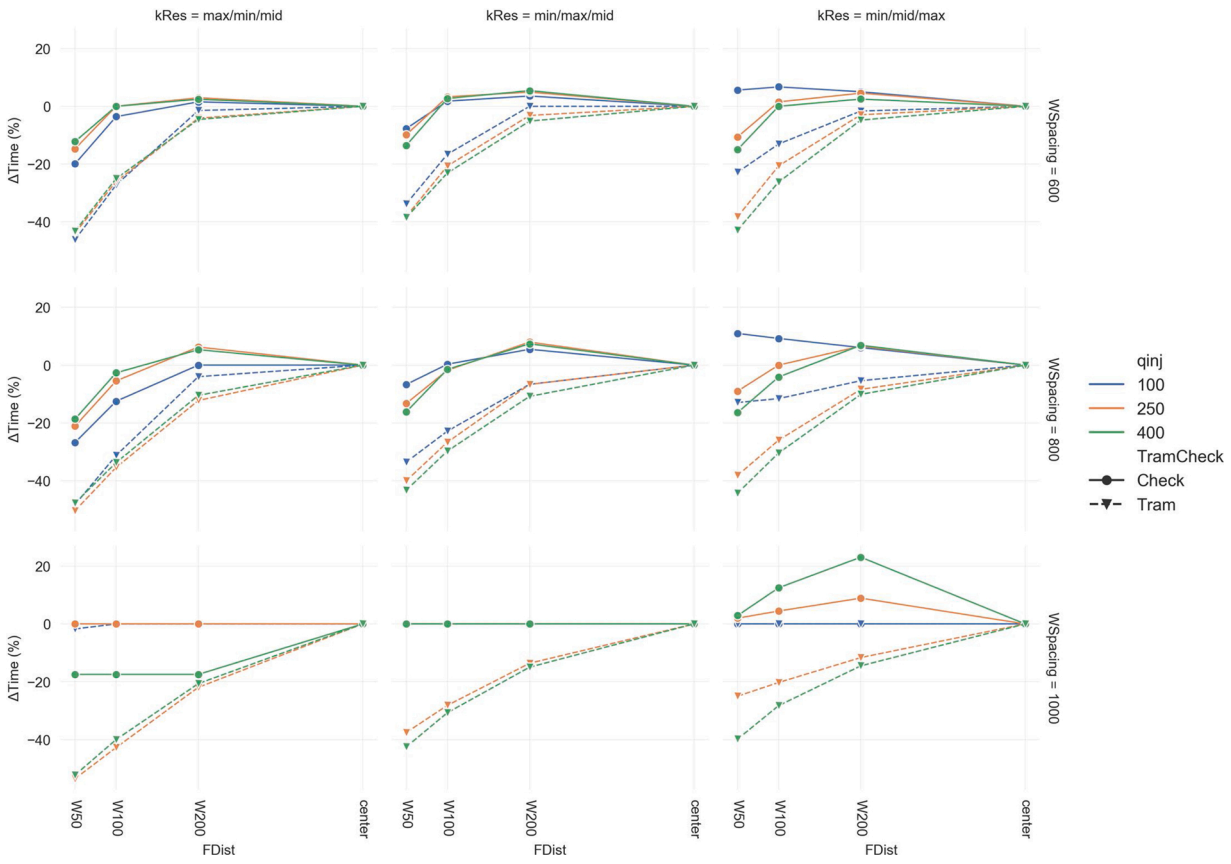

Fig. 13. Changes in system lifetime normalized to the fault positioned at the centre (0 %) for a single developer (mean temperature of both producing wells) for all the reservoir architectures and well spacing values, coloured by the production rate and market by the different well configurations. Data shown use a conduit fault permeability, a fault throw of 150 m and top west reservoir depth of 2.5 km.

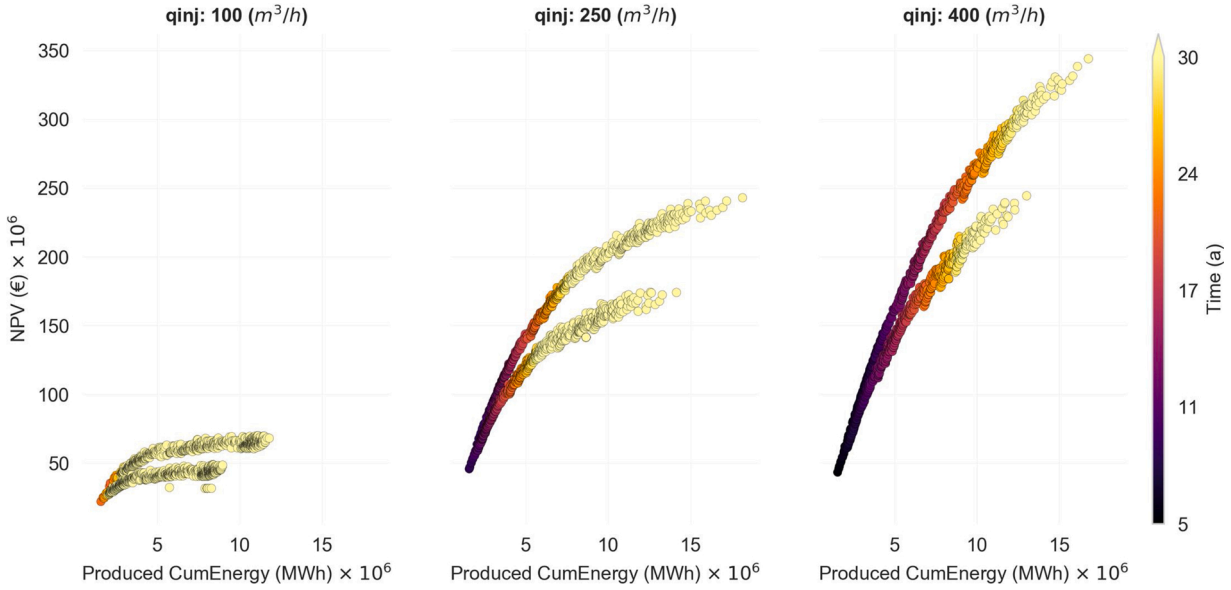

Fig. 14. Produced cumulative energy, NPV and system lifetime for a single operator of both doublets coloured by the time of thermal breakthrough. Data shown include the full dataset of 5184 simulations. The two different clouds per flow rate correspond to 2 km depth (lower NPV) and 2.5 km depth (higher NPV) resulting from higher temperatures with increasing depth due to the geothermal gradient. The scale is limited to 30 years, considered a reasonable project duration, to better highlight differences in lifetime for the different flow rates.

affected by the fault position since the only impact is the slightly larger reservoir volume available. Further increasing the rate to 400 m^3/h accentuates the difference between the tramline and checkerboard well configuration when the fault is positioned less than 200 m from the west doublet to circa 35 M€ and circa 50 M€ for the west and single developer accordingly.

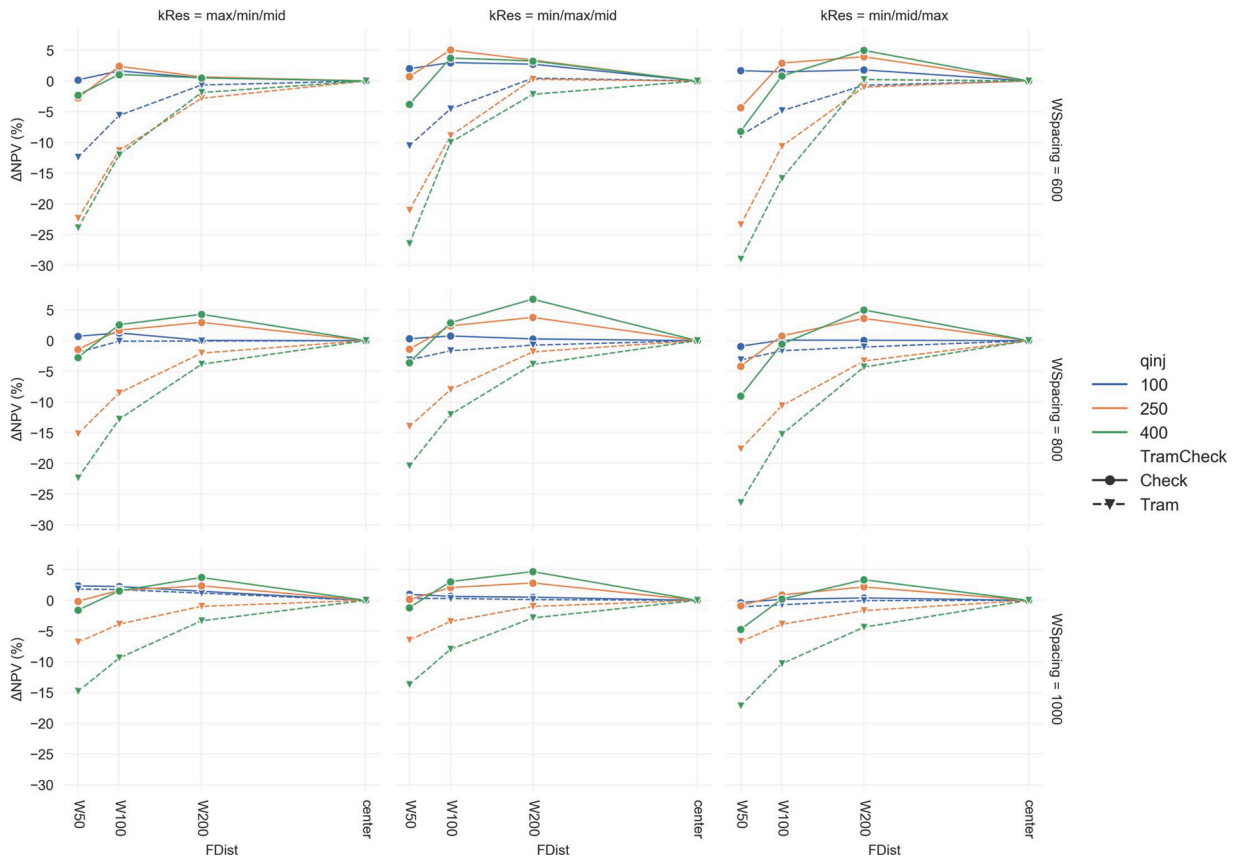

Fig. 15. NPV change normalized to the fault positioned at the centre (0%) for the single developer (mean temperature of both producing wells) for all the reservoir architectures and well spacing values, coloured by the production rate and market by the different well configurations. Data shown use a conduit fault permeability, a fault throw of 150 m and top west reservoir depth of 2.5 km.

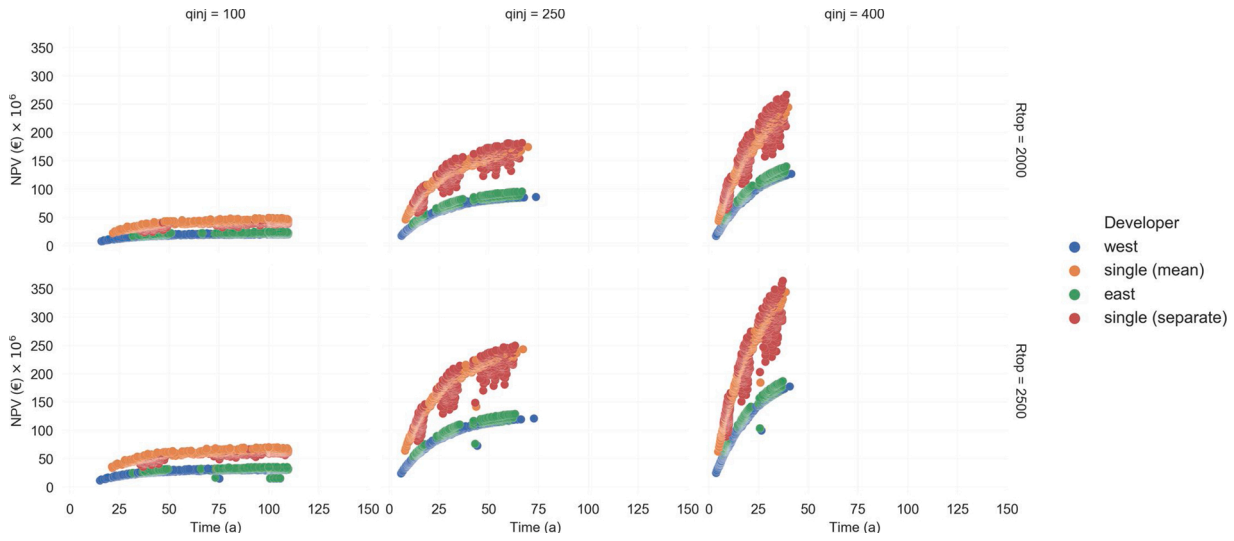

Fig. 16. NPV generated for single (mean), individual and single (separate) developers plotted against system lifetime. For the single developer, the operational strategy of using the mean temperature of both doublets can lead to both higher and lower NPV compared to a keeping each doublet separate.

A single developer operating the doublets separately benefits compared to a single developer using the mean temperature of both doublets when the high rate of 400 m^3/h is used (Fig. 19). With the fault positioned at the centre between the two doublets, the benefit is mostly in terms of NPV, as changes in lifetime are negligible. A sealing fault causes only minimal lifetime changes even as the west doublet is positioned closer to the fault. These positive changes are most pronounced for the large well spacing of 1000 m. With a transparent fault permeability and a distance of the west doublet to the fault less than 200 m changes in lifetime of more than 25 % are observed. The changes further increase with a conduit fault permeability. At the distance of 50 m from the west doublet a tramline configuration results in both higher lifetimes and NPV compared to the checkerboard configuration. Additionally, a shorter well spacing of 600 m achieves higher NPV changes despite the

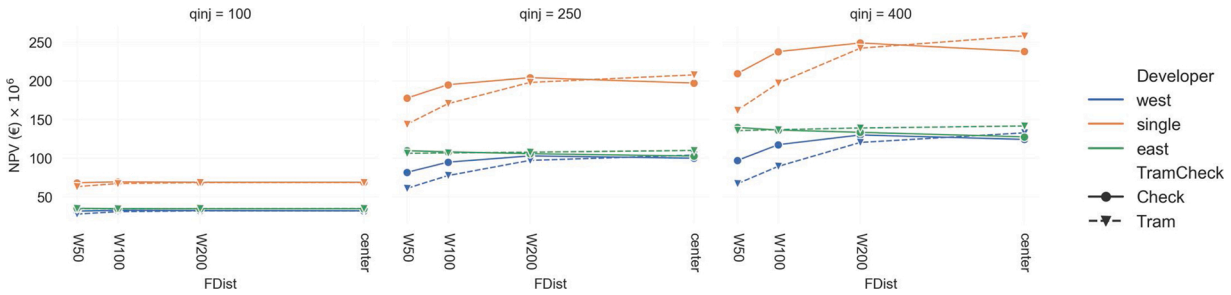

Fig. 17. Generated NPV for different developers and well configurations. Data shown use a well spacing of 800 m, a conduit fault permeability, a fault throw of 150 m, a top west reservoir depth of 2.5 km and a reservoir architecture of max/min/mid.

lower lifetime changes with respect to the large well spacing of 1000 m.

3.5. Energy recovery

The recovery of the HIP within the IA shows a perfectly linear behaviour that is a function of the production rate and the well spacing, with no influence from other parameters (Fig. 20). The production rate defines the speed of the recovery (see Fig. 20, secondary x-axis), while the well spacing affects both the speed but also the IA and therefore the areal extent over which recovery is calculated (see also Fig. 1b). For all rates, a shorter well spacing leads to higher energy recovery despite the shorter system lifetimes. With a rate of 100 m^3/h the system lifetime for the well spacing of 1000 m is in some cases longer than the 100 years of the simulation. For this rate, the highest HIP recovery of circa 43 % is achieved with a well spacing of 800 m. Some small deviations around the fit curve are observed for the low rates but as the rates are increased the fit becomes better. For the rate of 250 m^3/h and a well spacing of 600 m all simulations reach the system lifetime before 20 years but the highest recovery drops by circa 6% and it is notably faster compared to the rate of 100 m^3/h. All simulations with a rate of 250 m^3/h reach system lifetime within the 100 years of simulation and therefore the highest recovery of about 47 % is achieved with the well spacing of 1000 m. Increasing the rate to 400 m^3/h further shortens the system lifetime and increases the recovery rate, also leading to small decreases of the maximum achieved recovery for all three well spacings.

3.6. Influence area

Fig. 21 shows the temperature profiles while the 1 °C temperature drop reaches the IA boundary in the reservoir layer with the highest permeability for cases containing sealing faults, with various fault distance and flow rate values. For the rate of 100 m^3/h a minimum of 14 years of production takes place before the IA boundary is influenced by the cold front for a fault distance of 50 m and it increases to 25 years when the fault is in the centre of the two blocks. With a rate of 250 m^3/h, 6 and 10 years are needed respectively before the cold plume affects the IA boundary for a fault distance of 50 and 500 m respectively. These values are less than half compared to the lower rate of 100 m^3/h. A further decrease occurs with a rate of 400 m^3/h reducing the production time to less than a third compared to the respective values for the rate of 100 m^3/h. Consistently in all data shown in Fig. 21 the IA boundary is influenced by the cold water plume before any of the production wells is influenced.

The influence of the fault permeability to the 1 °C temperature drop is shown in Fig. 22 for the lowest rate of 100 m^3/h. A transparent fault permeability allows the cold front to reach the IA boundary at 11 years and a conduit fault at 8 years of production time. This further shortening of the production time before the IA boundary is influenced leads to an increased difference between the influence at the IA boundary and any of the production wells.

The discrepancy between the 1 °C temperature drop at the IA boundary and the production temperature of the single developer over the whole dataset suggests that the definition of the IA boundary is not suitable to link the temperature drop at the producer with that of the boundary (Fig. 23). For a rate of 100 m^3/h and short system lifetimes the discrepancy is small but increases substantially when longer system lifetimes are encountered reaching a maximum value of 86 years. For the rate of 250 m^3/h the discrepancy between the IA boundary and the production temperature is smaller for short system lifetimes and increases with longer system lifetimes up to circa 25 years. For the highest rate of 400 m^3/h and short system lifetime the discrepancy is further reduced and only reaches circa 17 years for the longest system lifetimes. Consistently throughout the dataset the ideal ratio of 1:1 between the IA boundary and the production temperature drop of 1 °C is not reached.

4. Discussion

In contrast to previously published work (Willems et al., 2017b), results herein show that for two doublets separated by a fault, with a doublet distance equal to the well spacing of both doublets a tramline configuration leads to longer lifetime for both doublets with the fault positioned at the centre. Previous results used a homogeneous reservoir and no fault was present between the two doublets, while in this study a layered reservoir with three layers is used and the two doublets are separated by a fault. Therefore, these different results in terms of well configuration could be attributed to either the reservoir layer properties or the fault presence. Longer lifetime however does not translate to improved NPV; these longer lifetimes are encountered beyond 30 years and therefore the time value of money minimizes the revenues from additional energy generation (see also Fig. 15).

Similar to our previous work for the effect of fault permeability and distance on a single doublet (Daniilidis et al., 2020a), also for interference between two doublets we observe significant effects when the doublet is positioned closer than 200 m from the fault. These effects are important for both the single and individual developers with the doublet closer to the fault being the most affected.

In agreement with previous research (Babaei and Nick, 2019), a well spacing of 1000 m is found to provide system lifetimes above 20 years in most cases, even when a high flow rate of 400 m^3/h is used. Reaching 30 or more years of system lifetime remains attainable, depending on the well configuration and reservoir architecture for a well spacing of 1000 m and 400 m^3/h. Notably, lifetimes above 20 years can also be achieved with a well spacing of 800 m and flow rate of 250 m^3/h or lower. Since typical projects span over some 30 years, current practice in terms of well spacing (circa 1.5 km, see also Table 1 in Willems and Nick, 2019) does not aid in the optimal use of the subsurface and could hinder the denser development required to increase DUGS contribution to the energy mix.

For the low rate of 100 m^3/h the NPV generated does not increase significantly when lifetime is extended beyond 30 years. A four-fold increase of rate to 400 m^3/h can result in an NPV increase of 5 times if sufficient lifetime is achieved. For the higher rates, no asymptotic behaviour is observed on the NPV meaning that further extending the lifetime will still yield economic benefit for the operator.

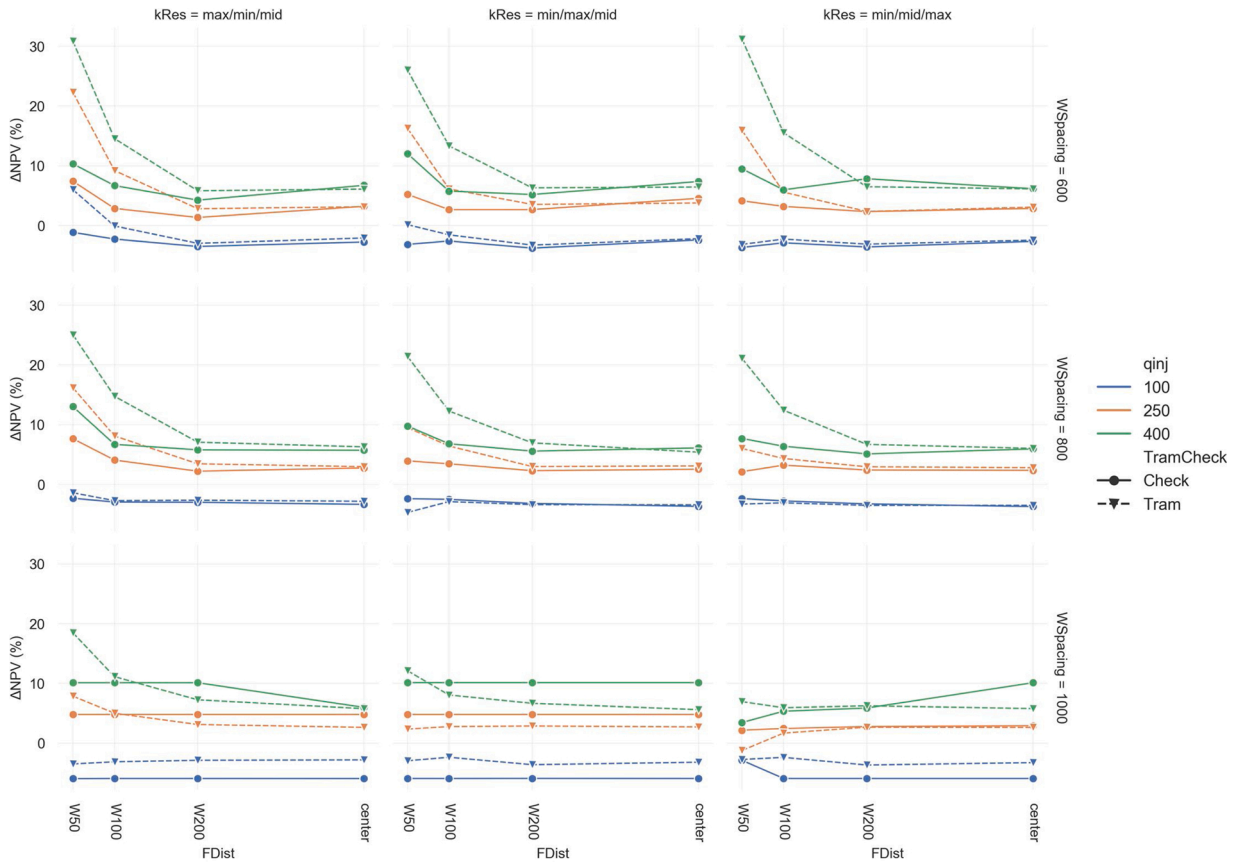

Fig. 18. NPV change of the west + east developer option with respect to single developer (0%) for a conduit fault, a fault throw of 150 m and a reservoir depth of 2500 m.

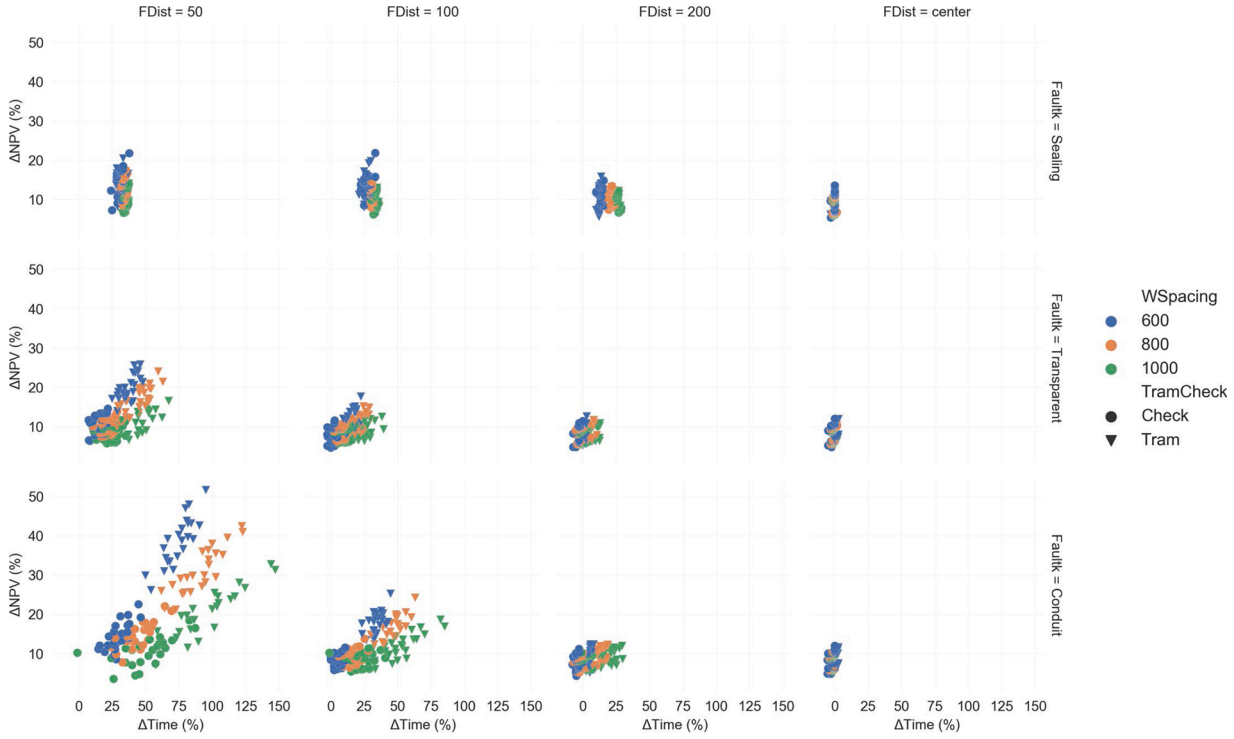

Fig. 19. Changes in system lifetime and NPV between a single developer (mean) (0,0) and a single developer (separate) for a flow rate of 400 m^3/h.

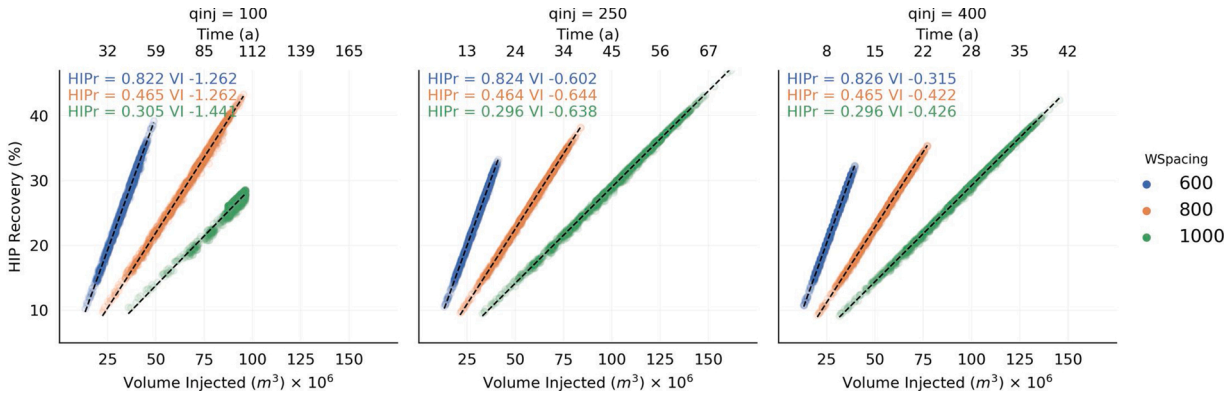

Fig. 20. Heat In Place (HIP) recovery as a function of volume injected (lower x-axis) and system lifetime (upper x-axis) for the different production rates and well spacing values. A linear fit is used on the data and the fit parameters are provided for each flow rate and well spacing combination.

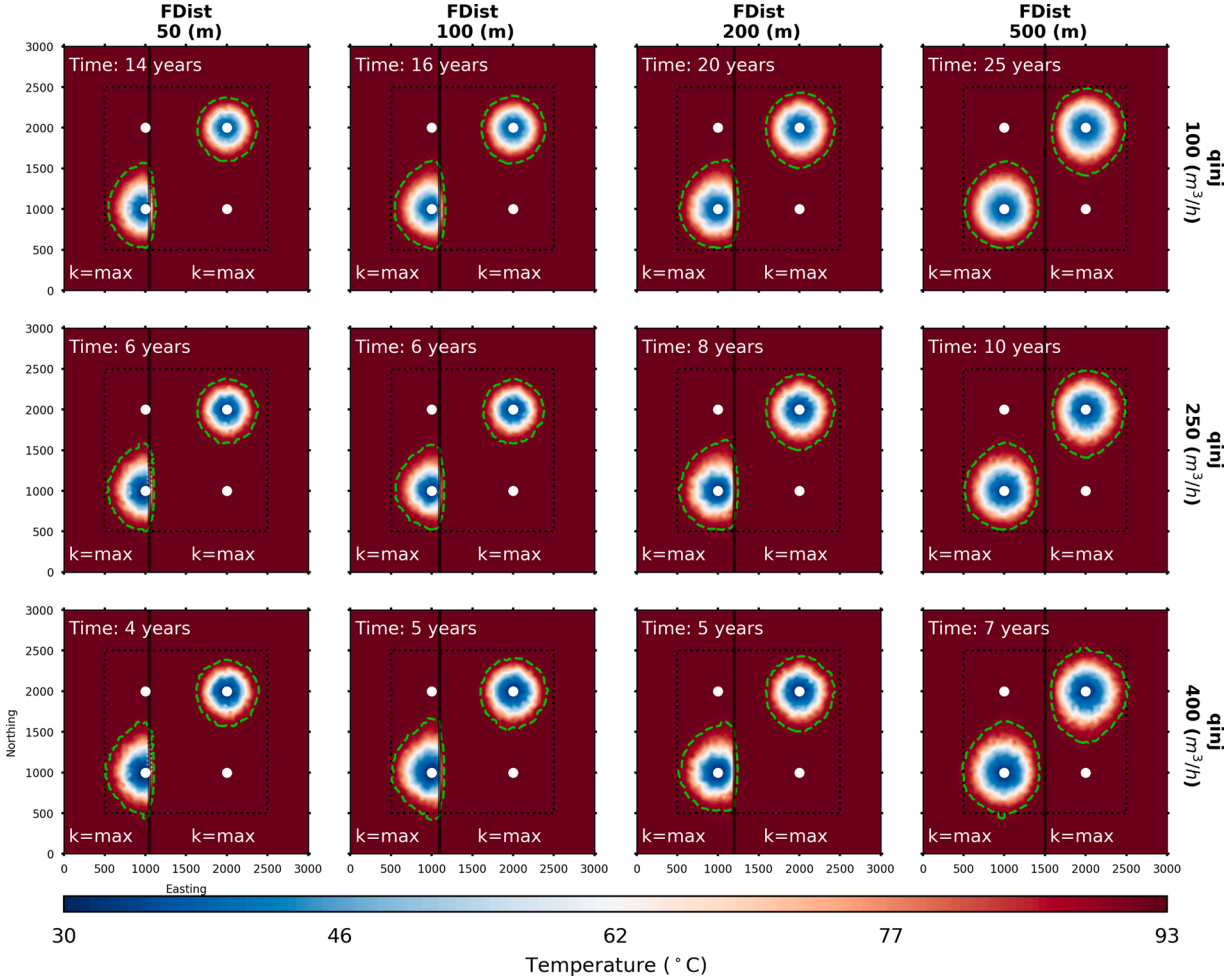

Fig. 21. Map view at the bottom of the west reservoir (depth of 2650 m) at the time that a 1 °C drop (lime contour) is observed at the IA boundary. The dataset shown is for checkerboard well configuration, well spacing of 1000 m, sealing fault, no fault throw, reservoir top at 2500 m, and a reservoir architecture of min/mid/max.

For a single developer using the mean temperature of both doublets always yields a higher NPV compared to operating the doublets separately for low rates. As the rates increase, operating the doublets separately can generate a higher combined NPV and longer systems lifetime; both NPV and lifetime benefits are increasing with lower well spacing and proximity to the fault. This can be attributed to the increasing discrepancy between the two doublets; the closer the west doublet is to the fault the earlier the thermal breakthrough and the lower its NPV will be. Therefore, a single developer using the mean temperature of both doublets will suffer from the earlier breakthrough of the west doublet being shorter. Operating the doublets separately is beneficial in this case as the maximum lifetime of each can be achieved. However, the drawback is that the power capacity of the system is limited to almost half once the west doublet has reached the end of its lifetime. Consequently, a regulator would prefer to steer development towards systems with multiple end-users to align with the increased economic value generated

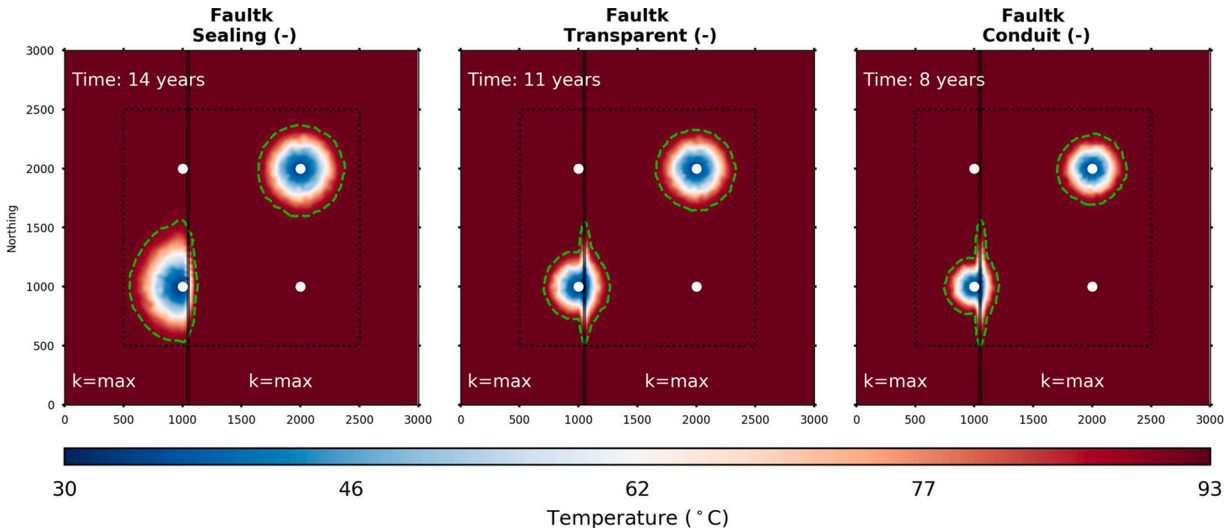

Fig. 22. Map view at the bottom of the west reservoir (depth of 2650 m) at the time that a 1 °C drop (lime contour) is observed at the influence boundary. The dataset show is for checkerboard well configuration, well spacing of 1000 m, flow rate of 100 m^3/h sealing fault, no fault throw, reservoir top at 2500 m, and a reservoir architecture of min/mid/max.

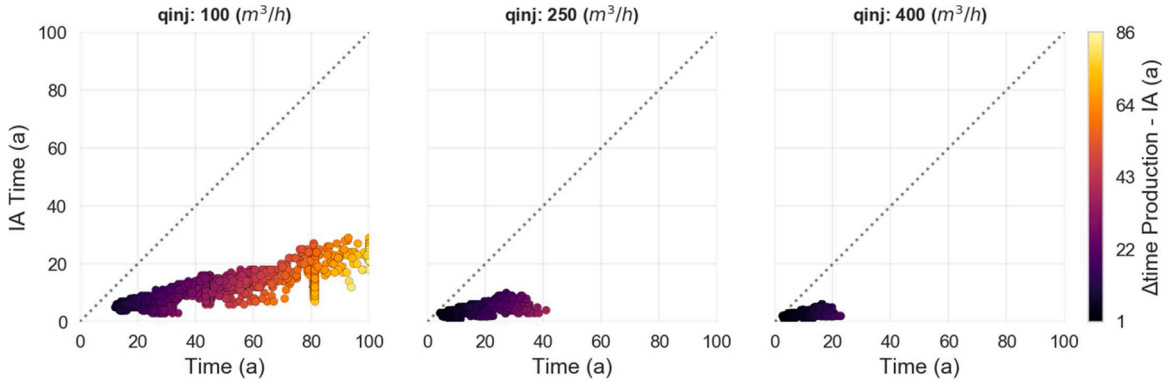

Fig. 23. Time of single developer production temperature drop of 1 °C (x-axis) to influence area (IA) time (y-axis) drop of 1 °C for the different flow rates considered. Data coloured according the difference between system lifetime and influence area time, dotted line represents a 1:1 ratio. Full dataset of 5184 simulations is shown.

from a single developer operating the doublets separately. Contrary to this, for a single developer with low rates (100 m^3/h) combining doublets to a system with higher capacity yields more profit (see also Fig. 18). The impact of the different development strategies for a single developer could be further explored considering options such as a staged addition of more doublets and a larger number of doublets overall. This however exceeds the scope of this work.

While proximity of the one doublet to the fault can reduce its lifetime, there are also positive effects that a permeable fault can have on both the lifetime and the NPV. This is also exemplified by the extensive flow field over the whole domain of the fault plane with a distance of 50 m to the west doublet for non-sealing fault behaviour (see also section 3.1 Flow field). Therefore, the distance to the fault plane can become a consideration in optimizing a development plan as it can result in lifetime increase of 20 % and an NPV increase of 5% in some cases (well spacing 1000 m, rate 400 m^3/h and maximum producing layer at the bottom, see Fig. 15).

In accordance with previously published work on the effect of fault proximity on a single doublet (Daniilidis et al., 2020a), the hydraulic effect of a fault is key for the interference between adjacent doublets. The fault hydraulic properties can have a decisive impact on the shape of the cold plume. The flow field shows a direct interaction between the two fault blocks when the fault acts as a conduit and a contribution from the whole fault extent, both vertically and laterally (see also section 3.1 Flow field). However, under all considered parameters, a checkerboard configuration is less affected by the fault behaviour compared to the tramline when all other parameters remain the same.

Considering field development and robustness, maintaining a distance of 200 m or more to the fault limits the fault effect to less than 20 % for the system lifetime and 5% of the NPV. Nonetheless, the checkerboard configuration is preferable when one doublet is closer to the fault and it is therefore preferable to use it in order to reduce the impact of the fault if the fault properties are not known.

Shorter well spacing results in better HIP recovery and the speed of the recovery is conditioned only to the well spacing and the production rate in a linear relationship. The well spacing plays a role since it defines the IA and therefore conditions the volume over which HIP recovery is calculated. It might therefore be worthwhile to examine if HIP recovery maintains such a linear relationship with respect to a different shape and dimensions of the IA. Regardless of the size and shape of the IA, decreasing the well spacing becomes increasingly important when dense development takes place and sweep efficiency is relevant. This is not only the case from the developer's point of view but also with respect to the efficient use of the subsurface resource.

Mechanical effects on the fault resulting from changes in both pressure and temperature around and inside the fault are not considered in this study. While this goes beyond the scope of this paper, preliminary results show that close proximity of the doublet to a fault can affect fault

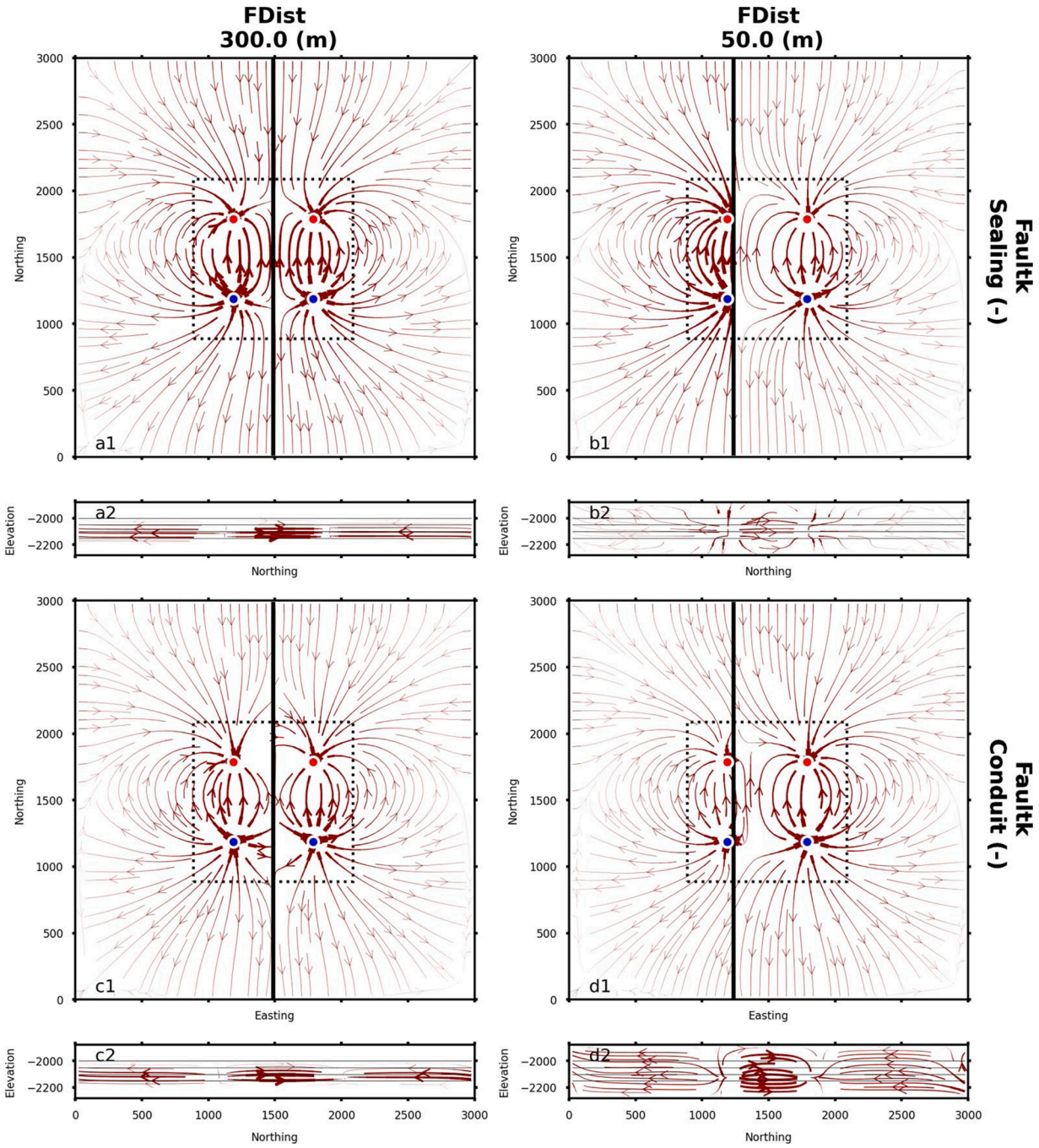

Fig. 24. Flow field at the base of the reservoir for a fault distance of 300 m (a1) and 50 m (a2) with a sealing fault and conduit fault respectively (c1 and d1) and their respective fault plane plots (a2,b2, c2, d2). Data shown use a checkerboard well configuration, a well spacing of 600 m, a fault throw of 0 m, a reservoir architecture of mid/min/max, a west reservoir top depth at 2 km and a flowrate of 400 m3/h. The dotted lines delineate the extent of the IA as defined in Fig. 1. The respective flow field for a tramline configuration can be found in Fig. 24.

stability (Zaal et al., 2021). Previous work has shown the temperature and pressure effects in lower dimension discontinuities such as fractures (Salimzadeh et al., 2019; Salimzadeh and Nick, 2019; Vik et al., 2018) also with the use of THM models (Li et al., 2019; Salimzadeh et al., 2018a). Thermal and hydraulic effects on open fractures have been shown to reduce fracture contact area and trigger fracture reactivation (Salimzadeh et al., 2018b). Moreover, coupled THM models have been used for high-enthalpy geothermal systems (Parisio et al., 2019; Watanabe et al., 2020). However, further research is to better constrain the mechanical effects of large faults in low-enthalpy, conduction dominated settings. Limited work has been directed to the combined analysis of the fault stability and field development in this context and this will gain increasing attention as denser developments materialize and interaction with faults becomes more frequent.

Discrepancy between IA temperature drop and drop at the producer wells increases with lower rates and longer system lifetimes. These findings are in accordance with Babaei and Nick (2019) where the IA needed to be expanded to capture the producer temperature drop. A different IA boundary needs to be designed as the production temperature is the only temperature that can be confidently measured in the field (IA temperature can only be simulated). An ideal IA would achieve 1:1 ratio between the IA boundary and the production temperature under all conditions, including heterogeneity at the reservoir, well spacing and the presence of a fault. This is a point for further study that

could enable a better planning and licensing of the subsurface for geothermal activities. A new IA should also be checked against the HIP recovery, which might change as the IA shape and dimensions change and constitutes a strong point for improvement of planning and regulation.

5. Conclusions

In this work a full factorial design was carried out to analyse the interference of two geothermal doublets across a fault using 5184 3D reservoir simulations. A synthetic, parametrizable model was used that considered subsurface parameters such as reservoir architecture, fault permeability, fault throw, fault distance to doublet and reservoir depth and development options such as well spacing, well configuration and flow rate. The system lifetime, generated energy, NPV, HIP recovery and IA boundary temperature were analysed for a single and individual developers. Based on the analysis the following conclusions can be drawn:

- Interference between doublets is affected primarily by the fault permeability and distance to fault and less so from the fault throw
- Interference of two doublets across a fault is minimized with the use of a checkerboard configuration. The benefits of the checkerboard configuration increase with fault proximity.
- Interference can conditionally be positive therefore the distance to fault should be included in field development optimization routines. Conditionality is subject to reservoir architecture, fault position and well spacing.
- A distance of at least 200 m from the fault ensures a lifetime change within 20 % and an NPV change within 5% compared to the fault at the centre between the two doublets.
- HIP recovery shows a linear relation with flow rate and well spacing. Higher rates and shorter well spacing result in faster HIP recovery.
- Shorter well spacing results in better HIP recovery and is therefore more effective for dense developments.
- A single developer of two doublets operating with mean temperature of both doublets can achieve approximately 5 times higher NPV for 4 times higher flow rate for similar amounts of produced energy compared to two individual developers, despite the lower system lifetime.
- Individual developers generate higher aggregated NPV compared to a single developer when the rates are 250 m^3/h or higher. This holds for both tramline and checkerboard configurations.
- A lifetime of more than 20 years can be attained with a well spacing of 1000 m and rate of 400 m^3/h; and for a well spacing of 800 m and a rate of 250 m^3/h or lower and the distance to the fault is larger than 200 m.
- The current definition of the IA is insufficient to capture the temperature drop at the producer wells. The discrepancy between the IA and the producer wells increases as system lifetimes become larger and as the fault permeability increases.

Availability of data and materials

The datasets used and/or analysed during the current study are available from the corresponding author on reasonable request.

Funding

This work has been funded by the Dutch Ministry of Economic Affairs and Climate Policy and ECW Netwerk BV under the research program Kennisagenda.

Conflict of interest and authorship conformation form

The authors have no affiliation with any organization with a direct or indirect financial interest in the subject matter discussed in the manuscript

CRediT authorship contribution statement

Alexandros Daniilidis: Conceptualization, Methodology, Software, Formal analysis, Investigation, Resources, Data curation, Writing - original draft, Writing - review & editing, Visualization, Project administration. **Hamidreza M. Nick:** Conceptualization, Methodology, Writing - review & editing, Funding acquisition. **David F. Bruhn:** Investigation, Writing - original draft, Writing - review & editing.

Acknowledgments

The authors would like to acknowledge the constructive feedback of Harmen Mijnlieff (TNO), Raymond Godderij (EBN), Bertran de Lange (ECW Netwerk) and Frank Schoof (Platform Geothermie) that helped shaping this work. Additionally, the authors are thankful to the reviewer and editor for the critical and constructive feedback that helped to improve the manuscript.

Appendix A

The main difference of the flow field with a tramline configuration with respect to a checkerboard configuration (Fig. 3) is the direction of the flow paths being parallel across the two sides of the fault plane.

Fig. 24

References

Alcalde, J., Bond, C.E., Johnson, G., Ellis, J.F., Butler, R.W.H., 2017. Impact of seismic image quality on fault interpretation uncertainty. GSA Today 27, 4–10. https://doi.org/10.1130/GSATG282A.1.

Anderson, A., Rezaie, B., 2019. Geothermal technology: trends and potential role in a sustainable future. Appl. Energy. https://doi.org/10.1016/j.apenergy.2019.04.102.

Babaei, M., Nick, H.M., 2019. Performance of low-enthalpy geothermal systems: interplay of spatially correlated heterogeneity and well-doublet spacings. Appl. Energy 253, 113569. https://doi.org/10.1016/j.apenergy.2019.113569.

Barbier, E., 2002. Geothermal energy technology and current status: an overview. Renewable Sustainable Energy Rev. 6, 3–65. https://doi.org/10.1016/S1364-0321(02)00002-3.

Bonté, D., van Wees, J.D., Verweij, J.M., 2012. Subsurface temperature of the onshore Netherlands: new temperature dataset and modelling. Netherlands J. Geosci. en Mijnb. 91, 491–515.

Botter, C., Cardozo, N., Hardy, S., Lecomte, I., Escalona, A., 2014. From mechanical modeling to seismic imaging of faults: a synthetic workflow to study the impact of faults on seismic. Mar. Pet. Geol. 57, 187–207. https://doi.org/10.1016/j.marpetgeo.2014.05.013.

Chen, M., Tompson, A.F.B., Mellors, R.J., Abdalla, O., 2015. An efficient optimization of well placement and control for a geothermal prospect under geological uncertainty. Appl. Energy 137, 352–363. https://doi.org/10.1016/j.apenergy.2014.10.036.

Chen, S., Zhang, Q., Li, H., Mclellan, B., Zhang, T., Tan, Z., 2019. Investment decision on shallow geothermal heating & cooling based on compound options model: a case study of China. Appl. Energy 254, 113655. https://doi.org/10.1016/j.apenergy.2019.113655.

Crooijmans, R.A., Willems, C.J.L., Nick, H.M., Bruhn, D.F., 2016. The influence of facies heterogeneity on the doublet performance in low-enthalpy geothermal sedimentary reservoirs. Geothermics 64, 209–219. https://doi.org/10.1016/j.geothermics.2016.06.004.

Daniilidis, A., Herber, R., 2017. Salt intrusions providing a new geothermal exploration target for higher energy recovery at shallower depths. Energy 118, 658–670. https://doi.org/10.1016/j.energy.2016.10.094.

Daniilidis, A., Doddema, L., Herber, R., 2016. Risk assessment of the Groningen geothermal potential: from seismic to reservoir uncertainty using a discrete parameter analysis. Geothermics 64. https://doi.org/10.1016/j.geothermics.2016.06.014.

Daniilidis, A., Alpsoy, B., Herber, R., 2017a. Impact of technical and economic uncertainties on the economic performance of a deep geothermal heat system. Renew. Energy 114, 805–816. https://doi.org/10.1016/j.renene.2017.07.090.

Daniilidis, A., Scholten, T., Hooghiem, J., De Persis, C., Herber, R., 2017b. Geochemical implications of production and storage control by coupling a direct-use geothermal system with heat networks. Appl. Energy 204, 254–270. https://doi.org/10.1016/j.apenergy.2017.06.056.

Daniilidis, A., Khait, M., Saeid, S., Bruhn, D.F., Voskov, D., 2020a. A High Performance Framework for the Optimization of Geothermal Systems, Comparing Energy Production and Economic Output, in: Proceedings World Geothermal Congress 2020. Reykjavik, Iceland, pp. 1–10.

Daniilidis, A., Nick, H.M., Bruhn, D.F., 2020b. Interdependencies between physical, design and operational parameters for direct use geothermal heat in faulted hydrothermal reservoirs. Geothermics 86, 101806. https://doi.org/10.1016/j.geothermics.2020.101806.

Daniilidis, A., Saeid, S., Gholizadeh Doonechaly, N., 2021. The Fault Plane As the Main Fluid Pathway: an Exploration of Field Development Options Under Uncertainty Based on the Rittershoffen Geothermal Field. Under Rev.

Faulkner, D.R., Rutter, E.H., 2001. Can the maintenance of overpressured fluids in large strike-slip fault zones explain their apparent weakness? Geology.

Garg, S.K., Combs, J., 2015. A reformulation of USGS volumetric "heat in place" resource estimation method. Geothermics 55, 150–158. https://doi.org/10.1016/J.GEOTHERMICS.2015.02.004.

Hoffmann, R., Dassargues, A., Goderniaux, P., Hermans, T., 2019. Heterogeneity and prior uncertainty investigation using a joint heat and solute tracer experiment in alluvial sediments. Front. Earth Sci.

Jalali, M., Embry, J.-M., Sanfilippo, F., Santarelli, F.J., Dusseault, M.B., 2016. Cross-flow analysis of injection wells in a multilayered reservoir. Petroleum 2, 273–281. https://doi.org/10.1016/J.PETLM.2016.05.005.

Li, S., Feng, X.T., Zhang, D., Tang, H., 2019. Coupled thermo-hydro-mechanical analysis of stimulation and production for fractured geothermal reservoirs. Appl. Energy. https://doi.org/10.1016/j.apenergy.2019.04.036.

Libak, A., Alaei, B., Torabi, A., 2017. Fault visualization and identification in fault seismic attribute volumes: implications for fault geometric characterization. Interpretation 5, B1–B16. https://doi.org/10.1190/INT-2016-0152.1.

Lund, J.W., Toth, A.N., 2020. Direct Utilization of Geothermal Energy 2020 Worldwide Review, in: World Geothermal Congress, pp. 1–39.

Malz, A., Madritsch, H., Kley, J., 2015. Improving 2D Seismic Interpretation in Challenging Settings by Integration of Restoration Techniques: a Case Study From the Jura Fold-and-thrust Belt (Switzerland). Interpretation 3, SAA37–SAA58. https://doi.org/10.1190/INT-2015-0012.1.

Parisio, F., Vilarrasa, V., Wang, W., Kolditz, O., Nagel, T., 2019. The risks of long-term re-injection in supercritical geothermal systems. Nat. Commun. 10, 1–11. https://doi.org/10.1038/s41467-019-12146-0.

Patel, D., Giertsen, C., Thurmond, J., Gjelberg, J., Gröller, M.E., 2008. The Seismic Analyzer: Interpreting and Illustrating 2D Seismic Data, in: IEEE Transactions on Visualization and Computer Graphics, pp. 1571–1578. https://doi.org/10.1109/TVCG.2008.170.

Saeid, S., Barends, F.B.J., 2009. An Extension of Lauwerier's Solution for Heat Flow in Saturated Porous Media, in: Proceedings of the COMSOL Conference. Milan.

Saeid, S., Nick, H.M., Barends, F., 2014. Experimental e numerical study of heat fl ow in deep low-enthalpy geothermal conditions. Renew. Energy 62, 716–730. https://doi.org/10.1016/j.renene.2013.08.037.

Saeid, S., Al-Khoury, R., Nick, H.M., Hicks, M.A., 2015. A prototype design model for deep low-enthalpy hydrothermal systems. Renew. Energy 77, 408–422. https://doi.org/10.1016/j.renene.2014.12.018.

Saeid, S., Wang, Y., Daniilidis, A., Khait, M., Voskov, D., Bruhn, D.F., 2020. Lifetime and Energy Prediction of Geothermal Systems: Uncertainty Analysis in Highly Heterogeneous Geothermal Reservoirs (Netherlands), in: Proceedings World Geothermal Congress 2020. Reykjavik, Iceland, pp. 1–8.

Salimzadeh, S., Nick, H.M., 2019. A coupled model for reactive flow through deformable fractures in enhanced Geothermal Systems. Geothermics 81, 88–100. https://doi.org/10.1016/J.GEOTHERMICS.2019.04.010.

Salimzadeh, S., Nick, H.M., Zimmerman, R.W., 2018a. Thermoporoelastic effects during heat extraction from low-permeability reservoirs. Energy. https://doi.org/10.1016/j.energy.2017.10.059.

Salimzadeh, S., Paluszny, A., Nick, H.M., Zimmerman, R.W., 2018b. A three-dimensional coupled thermo-hydro-mechanical model for deformable fractured geothermal systems. Geothermics. https://doi.org/10.1016/j.geothermics.2017.09.012.

Salimzadeh, S., Grandahl, M., Medetbekova, M., Nick, H.M., 2019. A novel radial jet drilling stimulation technique for enhancing heat recovery from fractured geothermal reservoirs. Renew. Energy. https://doi.org/10.1016/j.renene.2019.02.073.

Schoof, F., van der Hout, M., van Zanten, J., van Hoogstraten, J.W., 2018. Master Plan Geothermal Enrgy in the Netherlands.

Schulte, D.O., Arnold, D., Geiger, S., Demyanov, V., Sass, I., 2020. Multi-objective optimization under uncertainty of geothermal reservoirs using experimental design-based proxy models. Geothermics 86, 101792. https://doi.org/10.1016/j.geothermics.2019.101792.

TNO, 2018. ThermoGIS v2.0 - Economic Model [WWW Document]. ThermoGIS v2.0. URL https://www.thermogis.nl/en/economic-model (accessed 7.2.19)..

TNO-AGE, 2014. Bepaling Begrenzing Winningsvergunning Aardwarmte.

Vik, S.H., Salimzadeh, S., Nick, H.M., 2018. Heat recovery from multiple-fracture enhanced geothermal systems: the effect of thermoelastic fracture interactions. Renew. Energy 121, 606–622. https://doi.org/10.1016/J.RENENE.2018.01.039.

Wang, Z., Di, H., Shafiq, M.A., Alaudah, Y., Alregib, G., 2018. Successful leveraging of image processing and machine learning in seismic structural interpretation: a review. Proc. Int. Conf. Lead. Edge Manuf. 21st Century Lem21. https://doi.org/10.1190/tle37060451.1.

Watanabe, N., Saito, K., Okamoto, A., Nakamura, K., Ishibashi, T., Saishu, H., Komai, T., Tsuchiya, N., 2020. Stabilizing and enhancing permeability for sustainable and profitable energy extraction from superhot geothermal environments. Appl. Energy. https://doi.org/10.1016/j.apenergy.2019.114306.

Willems, C.J.L., Nick, H.M., 2019. Towards optimisation of geothermal heat recovery: an example from the West Netherlands Basin. Appl. Energy 247, 582–593. https://doi.org/10.1016/j.apenergy.2019.04.083.

Willems, C.J.L., Nick, H.M., Goense, T., Bruhn, D.F., 2017a. The impact of reduction of doublet well spacing on the Net Present Value and the life time of fluvial Hot Sedimentary Aquifer doublets. Geothermics 68, 54–66. https://doi.org/10.1016/j.geothermics.2017.02.008.

Willems, C.J.L., Nick, H.M., Weltje, G.-J., Bruhn, D.F., 2017b. An evaluation of interferences in heat production from low enthalpy geothermal doublets systems. Energy 135, 500–512. https://doi.org/10.1016/J.ENERGY.2017.06.129.

Yan, J., Chen, B., Wennersten, R., Campana, P., Yang, J., 2017. Cleaner energy for transition of cleaner city. Appl. Energy. https://doi.org/10.1016/j.apenergy.2017.04.015.

Zaal, C., Daniilidis, A., Vossepoel, F.C., 2021. Economic and Fault Stability Analysis of Geothermal Field Development in Hydrothermal Reservoirs. Submitted.